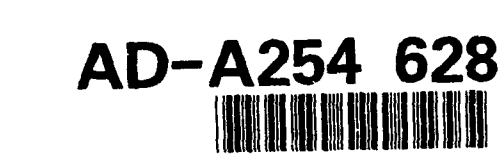

(2)

MICROSTRUCTURE-BASED FATIGUE LIFE PREDICTION METHODS FOR NAVAL STEEL STRUCTURES

Prepared By

K. S. Chan
D. L. Davidson
R. C. McClung

FIRST ANNUAL REPORT
July 15, 1991–July 15, 1992
SwRI Project No. 06-4414
ONR Contract No. N00014-91-C-0214

Submitted To

Office of Naval Research
800 N. Quincy Street
Arlington, VA 22217-5000

July 1992

SOUTHWEST RESEARCH INSTITUTE
SAN ANTONIO HOUSTON
DETROIT WASHINGTON, DC

REPORT DOCUMENTATION PAGE

Form Approved OMB No. 0704-0188 Exp.Date: Jun 30, 1986

1a. REPORT SECURITY CLASSIFICATION: Unclassified	1b. RESTRICTIVE MARKINGS
2a. SECURITY CLASSIFICATION AUTHORITY	3. DISTRIBUTION/AVAILABILITY OF REPORT: Unlimited
2b. DECLASSIFICATION/DOWNGRADING SCHEDULE	
4. PERFORMING ORGANIZATION REPORT NUMBER(S): 06-4414/1	5. MONITORING ORGANIZATION REPORT NUMBER(S)
6a. NAME OF PERFORMING ORGANIZATION: Southwest Research Institute; 6b. OFFICE SYMBOL (If applicable)	7a. NAME OF MONITORING ORGANIZATION: Office of Naval Research
6c. ADDRESS (City, State, and ZIP): 6220 Culebra Road, San Antonio, TX 78284	7b. ADDRESS (City, State, and ZIP Code): 800 N. Quincy Street, Arlington, VA 22217-5000
8a. NAME OF FUNDING/SPONSORING ORGANIZATION: Office of Naval Research; 8b. OFFICE SYMBOL (If applicable)	9. PROCUREMENT INSTRUMENT IDENTIFICATION NUMBER: N00014-91-C-0214
8c. ADDRESS (City, State, and ZIP): 800 North Quincy Street, Arlington, VA 22217-5000	10. SOURCE OF FUNDING NUMBERS: PROGRAM ELEMENT NO. / PROJECT NO. / TASK NO. / WORK UNIT ACCESSION NO.

11. TITLE (Include Security Classification): Microstructure-Based Fatigue Life Prediction Methods for Naval Steel Structures (First Annual Report)

12. PERSONAL AUTHOR(S): K. S. Chan, D. L. Davidson, and R. C. McClung

13a. TYPE OF REPORT	13.b TIME COVERED	14. DATE OF REPORT (Year, Month, Day)	15. PAGE COUNT
Technical	FROM 07/15/91 TO 07/15/92	92/07/15	50

16. SUPPLEMENTARY NOTATION

17. COSATI CODES			18. SUBJECT TERMS (Continue on reverse if necessary and identify by block number)
FIELD	GROUP	SUB-GROUP	Key Words: HSLA steels, fatigue life, fatigue crack growth, microcracks, fatigue damage, microstructure

19. ABSTRACT (Continue on reverse if necessary and identify by block number)

The goal of the subject program is to develop fundamental understandings of the relationships between microstructure and fatigue damage in structural steels of interest to naval applications. Quantitative descriptions of these relationships will be incorporated within practical engineering models for the prediction of *S-N* fatigue life. The focus of the first year of the program has been on experimental observations of fatigue damage in different microstructures for HSLA steels. Experimental methods were developed to study microcrack nucleation and growth with *S-N* fatigue specimens. Microstructures were modified with various heat treatments and characterized with appropriate optical and electron microscopy. The basic framework of potential microstructure-fatigue damage relationships has been sketched out.

20. DISTRIBUTION/AVAILABILITY OF ABSTRACT	21. ABSTRACT SECURITY CLASSIFICATION
☐ UNCLASSIFIED/UNLIMITED ☒ SAME AS RPT. ☐ DTIC USERS	Unclassified

22a. NAME OF RESPONSIBLE INDIVIDUAL	22b. TELEPHONE (Include Area Code)	22c. OFFICE SYMBOL
R. C. McClung	(512) 522-2422	

Table of Contents

ABSTRACT

The goal of the subject program is to develop fundamental understandings of the relationships between microstructure and fatigue damage in structural steels of interest to naval applications. Quantitative descriptions of these relationships will be incorporated within practical engineering models for the prediction of *S-N* fatigue life. The focus of the first year of the program has been on experimental observations of fatigue damage in different microstructures for HSLA steels. Experimental methods were developed to study microcrack nucleation and growth with *S-N* fatigue specimens. Microstructures were modified with various heat treatments and characterized with appropriate optical and electron microscopy. The basic framework of potential microstructure-fatigue damage relationships has been sketched out.

INTRODUCTION

The U.S. Navy currently employs HY-series steels in structural components such as submarine hulls. Since 1980, the Navy has also been evaluating the potential of HSLA (high-strength, low-alloy) steels for use in both ship and submarine construction. The introduction of these new steels has a complex impact on the design of naval structures. In some cases, design stress levels may increase to take advantage of improved properties under monotonic loading, but this could cause significant decreases in fatigue crack initiation and propagation lives. As a result, fatigue cracking could become one of the greatest threats to structural integrity in future pressure hulls operating at higher stress levels. On the other hand, the development of new alloys with new microstructures and new welding process specifications provides the opportunity to improve the fatigue resistance of the material and, ultimately, of the structure itself.

The subject program has been motivated by the desire for improved understandings of the relationships between microstructure and fatigue damage in naval steel structures, with particular application to the prediction of fatigue life. Among the intended products of the study are improved methods for fatigue life prediction which give appropriate attention to different potential microstructures and associated microstructural influences on initiation and/or growth rates. The methods could be used to provide guidance in optimizing alloy chemistry, processing, and welding protocols for improved fatigue resistance, while also facilitating improved fitness-for-service assessments of actual or postulated cracking.

Fatigue design for naval structures is currently most often based on the stress-life (S-N) approach which relates applied stresses directly to the total life to "failure". This approach enables the analyst to take a "black box" approach to fatigue design in which relatively little must be known about the actual fatigue damage processes. But fatigue "science", such as the study of microstructural influences on fatigue damage, must look "inside" the black box to identify and characterize the physical damage processes as much as possible. The total S-N life to "failure" is composed, in general, of three different life phases with specific physical damage processes: the nucleation of a

microcrack, the growth of this microcrack until it reaches some engineering size (often on the order of millimeters), and the subsequent growth of the large engineering crack to some definition of final failure. The total fatigue "life" is the sum of the lives associated with each phase. Under different conditions, one or more of the three phases may be dominant or negligibly small. For S-N fatigue life, which is typically characterized by the failure of a smooth axial or rotating bending fatigue specimen, the microcrack nucleation and growth phases are typically dominant. It is especially important to note that while S-N (smooth specimen) life is often thought of as an "initiation" life, a large fraction of the life may actually be expended in microcrack growth.

The focus of the first year of the subject program has been on experimental observations of fatigue damage in different microstructures for HSLA steels. Experimental methods were developed to study microcrack nucleation and growth with S-N fatigue specimens. Microstructures were modified with various heat treatments and characterized with appropriate optical and electron microscopy. The basic framework of potential microstructure-fatigue damage relationships has been sketched out.

MICROSTRUCTURES OF HSLA STEELS

Background

HSLA 80 and HSLA 100 steels are low-carbon, copper-bearing age-hardenable steels that possess a combination of high strength, high fracture toughness, and good weldability [1,2]. The former is the Naval designation [3] for ASTM A710 Grade A steels [4] modified to a military specification [3]. Typical compositions for HSLA 80 steels within the military specifications [3] are shown in Table 1. The HSLA 80 steel has low carbon (C < 0.06-0.07 wt.%) for good weldability, and a relatively high copper (1-1.3 wt.%) for precipitation strengthening [1].

A modified version of the A710 steel has been developed by increasing Mo and Mn contents [5] (Table 1). Because of high Mo and Mn contents, the modified A710 steel can be produced as thick plates with desirable combinations of strength and toughness that are not attainable in the center of A710 (or HSLA 80) thick plates [5]. HSLA 100 is a modification of HSLA 80 [2,3,6]; it contains the same alloying elements, but has greater amounts of nickel, copper, manganese, and molybdenum than HSLA 80. HSLA 100 has a minimum 690 MPa (100 ksi) yield strength and it can be solution-treated, quenched, and aged as HSLA 80.

Heat-treatment procedures for HSLA 80 steels follow a quenched and aged sequence similar to those for ASTM 710 Grade A, Class 3 steels. They involve austenitizing at 870° to 930°C (1600° to 1700°F) and water quenching to obtain a yield strength of about 450 MPa (65 ksi) [1-8]. Quenching after austenizing produces a very fine microstructure containing polygonal ferrite, accicular ferrite, and small amounts of lower-bainite and martensite/retained austenite [5,8,9]. The volume fraction of accicular ferrite increases with increasing cooling rate, while the volume fraction of polygonal ferrite increases with decreasing cooling rate [9]. The volume fractions of martensite and retained austensite are less than 3%, or 5% combined [9]. About 2% lower-bainite forms for cooling rates less than 2°C/s [9]. After quenching, ageing at 540° to 665°C (1000° to 1225°F) leads to the formation of ε-copper precipitates and a yield strength in excess of 552 MPa (80 ksi) due to precipitation hardening [5,8,9]. The precipitation of ε-copper in iron involves the initial formation of coherent, body-centered cubic, copper-rich clusters in ferrite [10]. These clusters, whose sizes are less than 5 nm in diameter, grow by bulk diffusion. These clusters lose coherency at approximately 5 nm, and eventually lead to the formation of ε-copper precipitates, whose sizes are in the range 5 to 50 nm [11].

The microstructures associated with the modified A710 and HSLA 100 steels are similar [6,12], but both are drastically different from that of conventionally heat-treated A710 or HSLA 80 steels. Austenitizing modified A710 [12] and HSLA 100 steels [6] at 900-915°C and water quenching results in a relatively coarse, aligned microstructure of ferrite laths and

Table 1
Composition of HSLA-80 Steels

Element	MIL-S-24645 (9/24/90)	DTNSRDC Plate #3	DTNSRDC GAH	DTNSRDC FXX	Lehigh Steel	
					Base Plate	Weld
C	.06	.07	.04	.04	.05	.06
Mn	.40/.70	*	.51	.55	.54	.95
Si	.40	.21	.31	.29	.27	.34
P	.020 max	*	.010	.010	.009	.013
S	.006 max	*	.009	.013	.001	----
Ni	.70/1.0	.76	.93	.83	.72	1.48
Mo	.15/.25	*	.20	.18	.196	.33
Cr	.6/.9	.7	.68	.78	.72	.55
V	.03	*	*	*	.005	*
Al	----	*	*	*	.047	*
Ti	.02	*	*	*	.005	*
Cu	1/1.3	.98	1.20	1.15	1.03	.68
Others	Ar, Su, Sb	*	Nb	Nb	*	*
Fe	Balance	Balance	Balance	Balance	Balance	Balance

* not determined

martensite/retained austenite as interlath particles in the as-quenched conditions. Like A710 and HSLA 80 steels, subsequent ageing of modified A710 and HSLA 100 steels in the 500° - 700°C causes precipitation of ε-copper precipitates [6].

The prevailing view in the literature is that microstructure exerts little effect on fatigue crack growth in the Paris (power-law growth) regime. For example, Braid and Knott [13] have observed little influence of grain size on fatigue crack growth in weldment of HY 80 steels when crack growth rates in fine-grained HAZ and coarse-grained HAZ materials were compared to the base material. In a different study, Hertzberg and Goodenow [14] observed some differences in fatigue crack growth behavior in a quenched and tempered steel and a vanadium HSLA steel (VAN-80). The former exhibited a tempered martensite microstructure and a 910 MPa yield strength, while the

latter exhibited a microstructure of ferrite plus pearlite, and a yield strength of 550 MPa. Since both the microstructure and yield strength were varied, the source responsible for the difference in crack growth behavior was not positively identified.

No information on the effects of microstructure on fatigue in HSLA steels has been reported in the literature. Compilation of fatigue crack growth data for A710 and HSLA 80 steels [2,5,7], shown in Figure 1, has revealed a relatively large variation in crack growth rates over a wide range of stress intensities for this class of steels. Since the microstructures for the steels shown in Figure 1 are not documented, it is not known whether the variation in crack growth rates is the result of microstructural influence, experimental scatter, test technique, or other factors. Available data from Lukens Steel for A710 [5], A710 modified [5], and HSLA 100 steels [15], however, indicate that the fatigue crack growth behaviors for these three steels are quite similar, as shown in Figure 2. Since the microstructures are quite different in these steels, the results in Figure 2 imply that microstructure exerts little or no influence on the crack growth behavior. This result is not surprising since all of the fatigue crack growth data reported are for through-thickness large cracks at stress intensities levels above the large-crack threshold.

Microstructural effects are expected to be most pronounced for large cracks in the near-threshold regime and for microcracks at stress intensities below the large crack threshold intensity, ΔK_{th}. With the exception of one study that examines the effect of grain size on ΔK_{th} [16], there have been no studies on the possible microstructural effects of fatigue crack initiation, the growth of microcracks and large cracks in HSLA steels for the near threshold region. Thus, there is a lack of understanding on microstructure/fatigue relationships in HSLA steels in general, and particularly in HSLA 80 and HSLA 100 steels. Research in this program in the first year is therefore focused on the effects of microstructure on the initiation and growth of microcracks in the HSLA 80 steel.

Heat-Treatment Procedures and Microstructures

Several 1-in. plates and 3/8-in. I-beams of HSLA 80 steels were obtained from David Taylor Naval Ship Research and Development Center (DTNSRDC) and Lehigh University, respectively. The HSLA 80 I-beams were fabricated by Bethlehem Steel and sent to Lehigh University via Ingalls Shipbuilding Inc., for use in a DTNSRDC-sponsored program on fatigue in HSLA structures. Because of common interest, the same HSLA 80 steels were chosen for studies at SwRI. Compositions of the HSLA steels from DTNSRDC and Lehigh University, shown in Table 1, were within naval specifications.

Research in the first year was focused on identifying the possible influence of microstructure on fatigue in HSLA steels. In particular, possible microstructural effects on initiation and growth of microcracks were examined. Two basic microstructures were of interest: (1) the polygonal and accicular ferrite microstructure typically found in HSLA 80 and A710 steels, and (2) the lath-like

microstructure commonly observed in the modified A710 and HSLA 100 steels. The former was the as-received microstructure in the HSLA 80 materials. The latter microstructure was achieved in the HSLA 80 steel through a heat-treatment procedure that involved austenitizing at 1200°C for one hour, followed by water quench and subsequent aging. This particular procedure was selected after a systematic screening of heat-treatment procedures and microstructures. Selected heat-treatment procedures and the resulting microstructures are presented in Table 2. The high austentizing temperature was selected in order to simulate the weld and HAZ conditions. Its selection was partly motivated by a previous study that indicated that lathlike ferrite formed in HSLA steels under high cooling rates [9].

Characterization of Microstructures

The microstructures of both the as-received and heat-treated materials were characterized by optical and transmission electron microscopies. Optical micrographs of the HSLA steel in the as-received, heat-treated (HT#2), heat-treated and aged (HT#3), and weld materials are presented in Figure 3, respectively. The as-received microstructure consisted mostly of fine polygonal and accicular ferrite grains with sulfide inclusions. The heat-treated materials exhibited a lath-like microstructure, which is similar to those observed in modified A710 and HSLA 100 steels. The weld microstructure, shown in Figure 3(d), appeared to contain coarse ferrite grains and small particles embedded within the ferrite grains. The nature of these embedded particles had not been identified.

In order to understand the relatively large variations in fatigue crack growth rates observed in Figure 2, two small pieces of HSLA 80 specimens (GAH and FZZ) were obtained from DTNSRDC. These specimens were also characterized for their microstructure. The microstructures of these two materials as revealed by optical microscopy consisted mostly of polygonal and accicular ferrites, as shown in Figure 4.

Transmission electron microscopy was also used to characterize the microstructures of the base material and weld of the HSLA steel. Precipitates on the order of 5 to 50 nm diameter in size were observed. Figure 5 shows these second phase precipitates in the as-received, heat-treated (HT#2), heat-treated and aged (HT#3), and weld materials, respectively. Morphologically, there appeared to be no significant differences in the precipitates observed in these four materials. These precipitates are probably mostly ε-copper, but some could be niobium carbonitrides [11]. No attempt was made to delineate the two types of precipitates. For comparison, TEM micrographs for the GAH and FZZ materials are shown in Figure 6, respectively. The size of the precipitates in the GAH material was similar to these observed in Figure 5 for the Lehigh material. On the other hand, the precipitate size in the FZZ material was much smaller than those for the GAH and Lehigh materials.

Table 2
Heat Treatments Used for Fatigue Specimens

No.	Plate Origin	Heat Treatment	Hardness
HT #1	Navy	900°C for 48 hrs., water quench, then 640°C for 0.5 hrs.	R_B 92
HT #2	Lehigh	1200°C for 1 hr., water quench.	R_C 26
HT #3	Lehigh	1200°C for 1 hr., water quench, then 593°C for 0.5 hrs.	R_C 31

The size distribution and volume fraction of the precipitates in the HSLA-steels were characterized using quantitative metallography. The measurement technique involved making a set of stereo-pairs of TEM micrographs of the representative microstructure. Precipitates in the TEM micrographs were traced on clear transparencies, which were then analyzed using a Tracor Image Analyzer to obtain the size distribution, the apparent area fraction, A′, and the mean precipitate diameter, d. The size distributions of ε-copper precipitates in the various microstructures of the Lehigh material are shown in Figure 7, while those for the GAH and FZZ materials are shown in Figure 8. A summary of the mean diameter and apparent area fraction, A′, is presented in Table 3.

To obtain the volume fraction of the precipitates using TEM micrographs, the thickness of the TEM foil must also be known. The thickness of the TEM foil was obtained by measuring the parallax displacement of a point at the top and bottom of the foil using a stereo-pair of TEM micrographs that were taken with different tilt angles, α. The foil thickness, t, was then computed according to [17]

$$t = \frac{p}{2\sin(\alpha/2)} \tag{1}$$

where p is the parallax displacement. The volume fraction, v_f, of the precipitates was then computed based on the expression [18]

$$v_f = -\left(\frac{2d}{2d+3t}\right)\ln(1-A') \tag{2}$$

which accounted for the contributions of overlapping precipitates to A′. Individual values of v_f for the various microstructures of the HSLA steel and weldment are presented in Table 3.

Table 3. Measurements of TEM foil thickness, t, mean diameter, d, apparent area fraction, A′, volume fraction, v_f, and free mean path, λ, of precipitates for HSLA 80 steels and welds.

Parameters	Spec 353 (As-Received)	Spec 357 (HT #2)	Spec 358 (HT #3)	Spec 359 (Weld)	GAH	FZZ
t (Å)	790	1700	920	1710	850	1120
d (Å)	122.2	121.1	126.2	105.5	174.8	66.4
A′ (%)	9.24	18.41	6.78	9.06	11.33	22.1
v_f (%)	0.91	0.92	0.59	0.38	1.45	0.95
λ (μm)	0.89	0.87	1.42	1.84	0.79	0.46

In addition to the ε-copper precipitates, the grain size and inclusion size distributions in the HSLA-80 base plate were also characterized. Low magnification optical micrographs were first obtained. The relevant microstructural features were then traced by outlining on clear transparencies with black markers. These images were subsequently processed using the Tracor Image Analyzer to obtain the mean diameter and size distribution profiles. Figures 9 and 10 show the size distribution of ferrite grains and sulfide inclusions for the HSLA 80 steel from Lehigh, respectively.

FATIGUE BEHAVIOR OF HSLA STEELS

Experimental Procedures

Small fatigue cracks were studied using two specimen designs. Initially, beams of square cross section 4 mm on a side by 52 mm long were loaded in 3-point bending. Stresses of increasing magnitude were applied until cracks were initiated within a few hundred thousand cycles. But the stresses required to initiate cracks were so high that the outer fiber stress exceeded yield, which meant the unloaded beam retained a permanent strain offset. The R-ratio (min. stress/max. stress) was maintained at nearly zero for the beam as a whole, but for the outer surface of the beam, the region in which the cracks started, $R \approx -0.33$ because of local plasticity. To overcome this difficulty, subsequent experiments were conducted using a rotating beam specimen, having the design shown in Figure 11, where the applied $R = -1$. Even with this specimen, the as-received material showed remarkable resistance to crack initiation, and the number of cycles required to initiate a crack were very sensitive to stress magnitude.

The surface preparation of specimens tested by these means is an important factor in setting the number of cycles to crack initiation. For this work, specimens were excised from the plates of material received using electric discharge machining (EDM). This machining method minimized residual stresses in the specimen surfaces and provided a good surface finish. The highly stressed regions of the specimens were hand polished by silicon carbide papers and finished by polishing with 0.1 μm diamond paste.

Plastic replicas were used to provide a history of the surface changes of all specimens due to cyclic loading. The maximum stress regions of the specimens were periodically replicated at half maximum load, and examined by optical microscopy after the plastic was rendered opaque by vacuum depositing silver on the replica surfaces. Replicas were made at the beginning of a test, with the specimen both unloaded and loaded, and then periodically until cracks were grown to approximately 2 mm in length. The number of cycles between replication was determined by the applied stress level and microstructure of the specimen. The number of cycles to crack initiation, the change in crack length with loading cycles, and the density of fatigue cracks initiated, were all determined from these replicas.

After the growth of the longest crack to about 2 mm, specimens were etched with 2% Nital and replicated. This was done in order to investigate the relationship between crack path and microstructure. None of the specimens tested had been broken into two pieces.

Results

An overview of the test results can be gained from examining how the number of cycles to initiation, N_i, and total number of cycles to grow the cracks to a length of 2 mm, N_f, varied as a function of stress. The relation between stress amplitude and N from the present tests, which encompasses a number of microstructures, is compared to previous work [1], which considered only the as-received microstructure, Figure 2. Data from the current work are comparable to previous results, and data from the rectangular beam specimens are comparable to those from the rotating beam specimens. Test results are listed in Table 4 for all the experiments conducted. The heat treatments shown in Table 4 by number are given in more detail in Table 2. Microstructure greatly affected the sites at which fatigue cracks initiated in this steel and the number of cracks that initiated. The microstructures tested are shown at low magnification in Figure 3, to give an overview of the various sizes of the features comprising each microstructure.

In the as-received microstructure (Lehigh material), Figure 3(a), cracks initiated from inclusions in almost every incidence. The size of the inclusions and their frequency of occurrence are shown in Figure 10, which is the result of the analysis of 86 inclusions. Inclusion size thus provides a lower limit to the smallest size of a crack that may be studied in this microstructure.

If the microstructure contained lath-like features, Figures 3(b) -(d), cracks no longer initiated at inclusions, but along the lath-like features instead. This shift in initiation site is illustrated in Figure 13. All parts of this illustration are at the same magnification, so it is possible to directly see the relationship between microstructural feature size and crack size near to the point of crack initiation.

A sequence of photographs made for crack growth from an inclusion initiated crack in as-received material is shown in Figure 14, Specimen 353. The crack initiated from one side of the inclusion but it grew approximately symmetrically—the initiating inclusion is marked by an arrow in Figure 14(d). Several cracks grown in this microstructure are shown in Figure 15, a SEM secondary electron image. These figures indicate that the trajectory of the crack path was not altered greatly as microstructural features were encountered during growth.

For cracks initiated in lath-like microstructures, the crack path was more affected by microstructural features, as shown in Figure 16. The crack shown in the figure initiated in the lath structure, not at an inclusion. Figure 16(d) was made after etching, and shows that the crack initiated in the center portion of one grain, and subsequent growth was in the lath direction until the crack reached a grain boundary; hence, crack growth to the left was across the lath direction of several small grains, while on the right, the crack grew more parallel to the laths. Similar behavior was exhibited by crack growth in another lath-like structure created by heat treatment, as shown in Figure 17. Lath direction is easily correlated with crack direction for this microstructure.

Table 4
HSLA-80 Fatigue Specimen Test Conditions

Spec. No.	Metall. Cond.	Spec. Type	Stress Amplitude (MPa)	N_i	N_f	R Ratio	Initiation Site
				-- cycles --			
346	As-Rec.	3-P	345	4.3×10^6	no cracks	0.1	---
347	As-Rec.	3-P	420	1.6×10^5	1.2×10^6	0.1	inclusions
350	HT #1	3-P	420	3.2×10^5	9.6×10^5	0.1	inclusions
353	As-Rec.	Ro-Bm	560	5.0×10^3	2.0×10^5	-1.0	inclusions
354	As-Rec.	Ro-Bm	520	4.0×10^4	3.2×10^5	-1.0	inclusions
357	HT #2	Ro-Bm	550	2.5×10^3	1.1×10^5	-1.0	laths
358	HT #3	Ro-Bm	520	3.5×10^4	1.9×10^5	-1.0	laths
359	Weld	Ro-Bm	520	5.0×10^3	1.6×10^5	-1.0	slip
360	As-Rec.	Ro-Bm	414	2.0×10^6	no cracks	-1.0	---
			448	1.5×10^6	no cracks	-1.0	---
			476	8×10^5	no cracks	-1.0	---

3-P = 3-point bending specimen; Ro-Bm = Rotating beam specimen.

Fatigue crack growth rates for the microstructures studied are shown in Figures 18-24. Crack length change, Δa, was measured at each end of the crack from replicas, and crack growth rate was calculated by dividing Δa by the number of cycles between replicas, ΔN. Periods when the crack was not growing are generally not shown. The minimum detectable crack growth rate, based on the resolution of the optical system used, was about 8×10^{-12} m/cycle. The cyclic stress intensity factor, ΔK, correlated with crack growth rate at cycle N was determined from half the total surface crack length, a, and the applied stress range, $\Delta\sigma$, using the relationship

$$\Delta K = 1.3\Delta\sigma\sqrt{a} \tag{3}$$

The information sought from these data are: (1) Whether or not there is a "small crack effect," i.e., do microcracks grow faster than large cracks for the same ΔK?; (2) Can microcracks grow at ΔK levels below the fatigue threshold for large cracks, ΔK_{th}?; and (3) What effect does microstructure have on the growth of microcracks?

The answers to these questions depend on several factors. To answer the first question, microcrack growth rate data are compared to large crack growth rate data; thus, the large crack growth rate data used are important. Most of the large crack growth rate data for the same as-received microstructure used here (Lehigh plate) do not extend below $\approx 10^{-8}$ m/cycle at this time, which complicates somewhat the comparison. However, when the microcrack growth rate data are compared to available large crack growth rate data, it appears that microcracks may grow slightly faster than would be anticipated from the large crack data. A more rigorous comparison will be completed when additional large crack data are available.

It is reasonably clear that microcracks do grow at values of ΔK below ΔK_{th} for large cracks. As will be shown in the next section, $5 < \Delta K_{th} < 10$ MPa$\sqrt{m}$ for most steels in this class. Since microcracks were found to grow at rates of $\approx 10^{-9}$ m/cy at ΔK values as low as 2 MPa$\sqrt{m}$, it is apparent that the answer to the second question is "yes."

The effects of microstructure on the growth rates of microcracks are less clear. The large scatter in crack growth rates makes it difficult to detect trends caused by microstructure. This scatter is partly related to the sampling rate used for measuring crack length. In general, the higher the resolution in measurement of crack length, the larger the scatter in crack growth rate. For large cracks, high resolution imaging of crack growth in the SEM, and by other methods, has shown that crack growth is intermittent and crack growth rates are highly variable. Smoothing of crack growth rate data may be accomplished by various techniques that are being explored now. The data of Figures 18-24 may be more easily interpreted, and the microstructurally based trends in growth rate better determined if smoothing of the data is systematically accomplished.

Growth rates of microcracks in the welded structure, Specimen 359, are affected by microstructure. This is illustrated more clearly in Figure 25 than in Figure 24. However, the usual interaction between microstructure and microcracks reported previously causes crack growth to be retarded by features like grain boundaries. For the weld microstructure the effect is opposite: crack growth is periodically accelerated. It may be that crack growth acceleration is due to the linking of several microcracks. Work is underway to examine the microstructural origins of this effect.

MODELING OF MICROSTRUCTURE/FATIGUE RELATIONSHIPS

Since most of the efforts in the first year had been focused on identifying the role of microstructure in fatigue of HSLA steels, only very limited work had been performed on developing the microstructure/fatigue relationships. The conceptual frame work for developing a deterministic, microstructure-based fatigue model for HSLA steels is outlined in Figure 26. The model is based on the separation of the total fatigue life into crack initiation and growth components. The initiation life model will be based on the Coffin-Manson low-cycle fatigue law, while the growth of small and large fatigue cracks will be treated with appropriate fatigue crack growth laws. The fatigue crack growth laws will include terms such as the yield stress, large-crack growth threshold, ΔK_{th}, and the critical stress intensity factor at fracture, K_{IC}. Most of the relations shown in Figure 26 are in functional or empirical forms. The goal of this program is to develop the microstructure-based fatigue model using the micromechanical approach so that empirical constants are kept to a minimum.

Many of the microstructure/property relationships shown in Figure 26 are based on the grain size, inclusion size, and the mean free path of the second phase. Experimental results of these quantities will be used in the model development for HSLA steels. However, it is preferable that some of these quantities be calculated based on compositions so that laborious quantitative measurements need not be repeated in the future. One such microstructural parameter is the volume fraction, v_f, of the ε-copper. A simple analysis developed in this program based on phase equilibrium leads to

$$v_f = \frac{\rho_{Fe}}{\rho_{cu}} \frac{(X_{cu} - X_o)}{(100 - X_{cu})} \times 100\% \qquad (4)$$

as the volume fraction of ε-copper expected for Fe as functions of copper content, X_{cu}, in wt. %, the solubility of copper, X_o (in wt. %), in iron at ambient temperature, and density, ρ. Comparison of Eq. (4) and experimentally measured volume fraction of ε-copper in HSLA steels from this study and the literature [8,10,18] is shown in Figure 27. The good agreement suggests that Eq. (4) might be used for estimating the value of v_f based on copper content. Once v_f is known, the mean free path, λ, for the ε-copper precipitate can be evaluated according to [19]

$$\lambda = \frac{2d(1 - v_f)}{3v_f} \qquad (5)$$

where d is the average diameter of the ε-copper precipitates. The values of the mean free path for ε-copper precipitates in the various microstructures studied are presented in Table 3. Both the grain size and the precipitate mean free path are required in the σ_y, K_{IC}, and possibly ΔK_{th} expressions.

Available ΔK_{th} data for HSLA steels [16], shown in Figure 28, indicate that the growth threshold, ΔK_{th}, increases with grain size, D, according to the relation given by

$$\Delta K_{th} = \Delta K_o + \sigma_{ys}\sqrt{2\pi D} \tag{6}$$

where ΔK_o is a component of ΔK_{th} that is independent of grain size. The second term in Eq. (6) is reminiscent of: (1) the ΔK_T expression due to Yoder, et al. [20], for the transition of microstructure-sensitive to microstructure-insensitive fatigue crack growth in $\alpha + \beta$ Ti-alloys; and (2) the ΔK_{th} expression,

$$\Delta K_{th} = \sigma_{ys}\sqrt{2\pi r_s} \tag{7}$$

suggested by Davidson [21] for a growth threshold originated from the need to activate slip over a distance, r_s, ahead of the crack tip, where r_s is the slip line length. The second term of Eq. (6) can be obtained from Eq. (7) by assuming the dominant obstacle is the grain boundaries and equating r_s to the grain diameter, D. The $\Delta K_{th} \propto \sigma_y\sqrt{D}$ relation observed in Figure 28 has also been explained on the basis of roughness-induced crack closure [22] by Gerberich, et al. [16]. In this case, the grain size dependence arises from crack closure due to contacts of the fracture surface asperities at a distance on the order of the grain size, D, behind the crack tip. Recent theoretical analyses by Ravichandran and Dwarakadasa [23] suggested that ΔK_{th} for large cracks may arise from a cleavage term, a slip term, and a roughness-induced closure term. The cleavage term is independent of grain size, while both the slip and roughness-induced closure terms are proportional to $\sigma_y\sqrt{D}$. Thus, it is possible that ΔK_{th} in HSLA steels can arise from a grain-size independent term and a grain-size dependent term. The latter can originate from either slip or roughness-induced closure. At the present time, the mechanism responsible for ΔK_o is not known. It is unclear whether or not ΔK_o arises from cleavage.

One possible microstructural effect has been identified for fatigue crack growth in HSLA steels. Recall that in the power-law regime, the fastest crack growth rate among the HSLA 80 shown in Figure 1 is the FZZ steel, while the slowest corresponds to the GAH steel. Comparison of microstructure and fatigue crack growth behavior for these two steels in Figure 29 reveals that the higher crack growth rate in FZZ is associated with fine precipitates, while the slower crack growth rate in GAH is associated with larger precipitates. The difference in precipitate sizes is consistent with a higher strength, but lower toughness, for the FZZ steel. Assuming that the precipitates in FZZ and GAH are both ε-Cu precipitates, this result suggests that fatigue crack growth in HSLA steels is somewhat sensitive to the size and distribution of precipitates. This microstructural effect will be incorporated into the fatigue crack growth model to be developed in this program.

Results obtained in this study indicated that fatigue crack growth rates of microcracks in HSLA steels are only mildly dependent on microstructure. Figure 30 shows the approximate central tendencies of microcrack growth rates for four microstructures (without the more rigorous smoothing and statistical analysis currently underway). The relatively small effects of microstructure on fatigue crack growth of microcracks are consistent with the large crack results shown in Figure 2 for A710, A710 modified, and HSLA steels. In both figures, crack growth rates for materials with the polygonal and accicular ferrite microstructure (typical of HSLA 80 and A710 steels) are compared with the lath-like microstructure (typical of A710 modified and HSLA 100 steels. The ramification of the results shown in Figures 2 and 30, and that in Figure 29, is that fatigue crack growth rate in these steels is insensitive to the morphology of the ferrite matrix, but is affected by size, volume fraction, and possibly the mean free path of the ε-copper precipitates. Since the copper content in these steels is specified to within a small range (1 to 1.3 wt. %), the microstructural parameters pertaining to the precipitates accordingly also lie within a small range and then, therefore, result in only small variations of crack growth rate with microstructure, as observed in Figures 1, 2, 29, and 30.

DISCUSSION AND FUTURE WORK

The results to date have successfully demonstrated one of the fundamental premises of the research plan: that S-N fatigue life for naval structural steels can be adequately characterized in terms of the nucleation and growth of individual microcracks. Although none of the specimens were cycled to complete fracture, the predicted remaining life after the longest crack reaches about 2 mm (the "failure" criterion used here) is typically on the order of a few thousand cycles, a negligible number in comparison to the recorded N_f values. Furthermore, for the applied stresses considered to date, the reported microcrack nucleation life (N_i in Table 4) is typically a very small fraction of the total life (on the average, around 0.1 N_f, and sometimes much smaller). Since these results are for highly polished smooth specimens, it is likely that actual initiation lives in many applications, where surface finishes will be inferior, would be even smaller fractions of total life.

The most important fatigue damage mechanisms for S-N fatigue life under these conditions, therefore, are typically those associated with microcrack growth. A rigorous description of microcrack growth should be sufficient to describe both central tendencies and variability in total S-N fatigue life. To date, this has been shown in principle. As specific microcrack growth models are developed in future work, however, it should be possible to integrate these models and obtain specific quantitative estimates of total life (i.e., construct the S-N curve). And important effects on total S-N life, such as microstructural or environmental influences, should be explainable in terms of the fatigue damage processes associated with microcrack growth.

The potential importance of the microcrack nucleation phase should not be *a priori* ruled out, however. At slightly lower stress levels, near or below the endurance limit, the nucleation phase is expected to be a larger fraction of total life (as evidenced, at least in part, by the absence of nucleated microcracks after 4×10^6 cycles in Specimen #360, Table 4). In addition, the clearest microstructural effects on fatigue damage observed to date were associated with microcrack nucleation: the change in nucleation site with different heat treatments, and the identification of specific microstructural features (such as inclusions) with nucleation sites. It is reasonable to postulate, for example, that variations in inclusion size could be directly linked to variations in nucleation life for the as-received material condition.

The microcrack growth data presented in this report are actually still "raw" data awaiting further analyses. First of all, comparisons of microcrack growth rates from different specimen geometries and comparisons with traditional "large" crack growth rate data will require modification of the baseline ΔK values to ΔK_{eff} through appropriate determination of crack closure levels. We are also awaiting the necessary large crack growth rate data for the same heat of material from tests currently being conducted at Lehigh. These data and analyses, along with further smoothing of the existing data, must be completed before final conclusions can be drawn about microstructural influences or about large vs. small crack growth rates.

In related work planned for the coming contract year, we will perform probabilistic analyses of the microcrack growth data. Our goals are to link the observed variability in microcrack growth rates to variability in the factors which influence the fatigue damage process, such as microstructure, and (ultimately) to variability in total S-N fatigue life.

As noted previously, it appears from investigations conducted to date that microcrack growth rates in HSLA steels are only mildly dependent on microstructure. The most significant potential effect discovered is a possible link between crack growth rate and the size and distribution of fine copper precipitates. We will conduct additional experimental investigations in the coming year in attempts to alter the precipitate size via heat treatment and conduct appropriate fatigue tests.

REFERENCES

1. T.W. Montemarano, B.P. Sack, J.P. Gudas, M.G. Vassilaros, and H.H. Vanderveldt, *J. of Ship Production*, Vol. 2, No. 3, 1986, pp. 145-162.

2. T.W. Montemarano, R.T. Brenna, T.E. Caton, D.A. Davis, R.L. McGaw, L.J. Roberson, T.M. Scoonover, and R.J. Wong, DTNSRDC TM-28-84-17, David W. Taylor Naval Ship Research and Development Center, 1984.

3. MIL-S-24645A (SH), Amendment 1, Naval Sea Systems Command, Department of the Navy, Washington, DC, September 24, 1990.

4. ASTM A710/A710M-85a, in 1987 Annual Book of ASTM Standards, Vol. 01.04, pp. 664, *ASTM*, Philadelphia, PA, 1987.

5. A.D. Wilson, C.R. Roper, Jr., and E.G. Hamburg, SAE Paper 870790, 1988, pp. 2.1127-2.1146.

6. M.H. Heinze, MS Thesis, Naval Postgraduate School, Monterey, CA, 1988.

7. J.A. Todd, P. Li, G. Lin, and V. Ramon, *Scripta Metall.*, Vol. 22, 1988, pp. 745-750.

8. R.J. Jessman and G.J. Murphy, *J. Heat- Treating*, Vol. 3, No. 3, 1984, pp. 228-236.

9. G.R. Speich and T.M. Scoonover, in Processing, Microstructure, and Properties of HSLA Steels, edited by A.J. DeArdo, *AIME-TMS*, Warendale, PA, 1988, pp. 265-287.

10. S.R. Goodman, S.S. Brenner, and J.R. Low, Jr., *Metall. Trans. A*, Vol. 4, 1973, pp. 2363-2369.

11. M.T. Miglin, J.P. Hirth, A.R. Rosenfield, and W.A.T. Clark, *Metall. Trans. A*, Vol. 17A, 1986, pp. 791-798.

12. S.W. Thompson, D.J. Colvin, and G. Krauss, *Script Met.*, Vol. 22, 1988, pp. 1069-1074.

13. J.E.M. Braid and J.F. Knott, in Advances in Fracture Research '81, edited by D. Francosi, Pergamon Press, Oxford, U.K., Vol. 5, 1981, pp. 2061-2069.

14. R.W. Hertzberg and R.H. Goodenow, in Microalloying 75, Union Carbide, Niagara Falls, NY., 1981, pp. 503-516.

15. A.D. Wilson and E.G. Hamburg, Lukens Steel Report No. RQRAD9-1, 1989.

16. W.W. Gerberich, W. Yu, and K. Esaklul, *Metall. Trans. A*, Vol. 15A, 1988, pp. 875-888.

17. A. Boyde, in Scanning Electron Microscopy/1979/II, SEM Inc., *AMF*, O'Hare, IL, 1979, pp. 67-78.

18. J.J. Aroztegui, J.J. Urcola, and M. Fuenntes, *Metall. Trans. A*, Vol. 20A, 1989, pp. 1657-1668.

19. J.W. Martin, Micromechanisms in Particle Hardened Alloys, Cambridge Univ. Press, 1980, pp. 43.

20. G.R. Yoder, L.A. Cooley, and T.W. Crooker, in Titanium 80, H. Kimura and O. Izumi, eds., *TMS-AIME*, Warrendale, PA, 1981, Vol. 3, pp. 1865-1875.

21. D.L. Davidson, *Acta Metall.*, Vol. 36, 1988, pp. 2275-2282.

22. R.O. Ritchie and S. Suresh, *Metall. Trans. A*, Vol. 13A, 1982, pp. 937-940.

23. K.S. Ravichandran and E.S. Dwarakadasa, *Acta Metall.*, Vol. 39, 1991, pp. 1343-1357.

ACKNOWLEDGEMENTS

The support of ONR Scientific Officer A. K. Vasudevan is gratefully acknowledged. The authors extend their thanks to A. Nagy for help in specimen machining and use of the equipment for the rotating beam tests; to B. K. Chapa for careful and dedicated performance of experiments and measurements of crack initiation and growth; and to Y.-M. Pan for excellence in performing the TEM investigations.

FIGURES

Figure 13. The relationship between microstructure and crack initiation sites: (a)-(d) show microcracks near initiation; (e)-(h) show microstructures of the same scale as the upper photographs. (a) and (e) as-received microstructure; (b) and (f) HT#1, sp. 350 (to cause grain growth); (c) and (g) HT#2, sp. 357, and (d) and (h) HT#3, sp. 358.

Figure 14. Crack initiation and growth sequence, as-received, sp. 353. (a) 20 kcy, (b) 30 kcy, (c) 70 kcy and (d) 170 kcy.

Figure 15. Crack path in relation to microstructural features. (a,b) as-received (Navy plate), (c,d) sp. 347, as-received (Lehigh plate), (e,f) sp. 353, and weld, sp. 359.

Figure 16. Crack initiation and growth sequence, HT#3, sp. 358: (a) 70 kcy, (b) 140 kcy, (c) 180 kcy, and (d) 180 kcy after etching. Stress axis vertical.

Figure 17. Crack path in relationship to microstructure, HT#2, sp. 357 after 110 kcy. Before and after etching. Stress axis vertical.

Figure 18. Fatigue crack growth rate for as-received material (Navy plate) from 3-point bend bar test, sp. 347.

Figure 19. Fatigue crack growth rate for HT#1 (Navy plate) from 3-point bend bar test, sp. 350.

Figure 20. Fatigue crack growth rate for as-received material (Lehigh plate) from rotating beam test, sp. 353, stress amplitude = 550 MPa.

Figure 21. Fatigue crack growth rate for as-received material (Lehigh plate) from rotating beam test, sp. 354, stress amplitude = 520 MPa.

Figure 22. Fatigue crack growth rate, rotating beam test, for sp. 357, HT#2.

Figure 23. Fatigue crack growth rate, rotating beam test, for sp. 358, HT#3.

Figure 24. Fatigue crack growth rate, rotating beam test, for sp. 359, weld metal.

Figure 25. Weld metal specimen 359—comparison of the changes in crack length and crack growth rate as a function of loading cycles. Arrows indicate locations where cracks growth rate accelerated.

Figure 26. Flow chart showing the approach for developing microstructure\fatigue relationships for HSLA steels.

Figure 27. Theoretical and experimental results of volume fraction of ε-copper precipitates as a function of copper content in steels. The experimental results are from this study, Aroztegui, et al. [18], and Goodman, et al. [10].

Figure 28. Theoretical and experimental relations between ΔK_{th} and $\sigma_{ys}\sqrt{D}$.

Figure 29. Dependence of fatigue crack growth rate on the size of ε-copper precipitates in FZZ and GAH plates.

Figure 30. Comparison of fatigue crack growth responses of microcracks in HSLA 80 steels and weld.

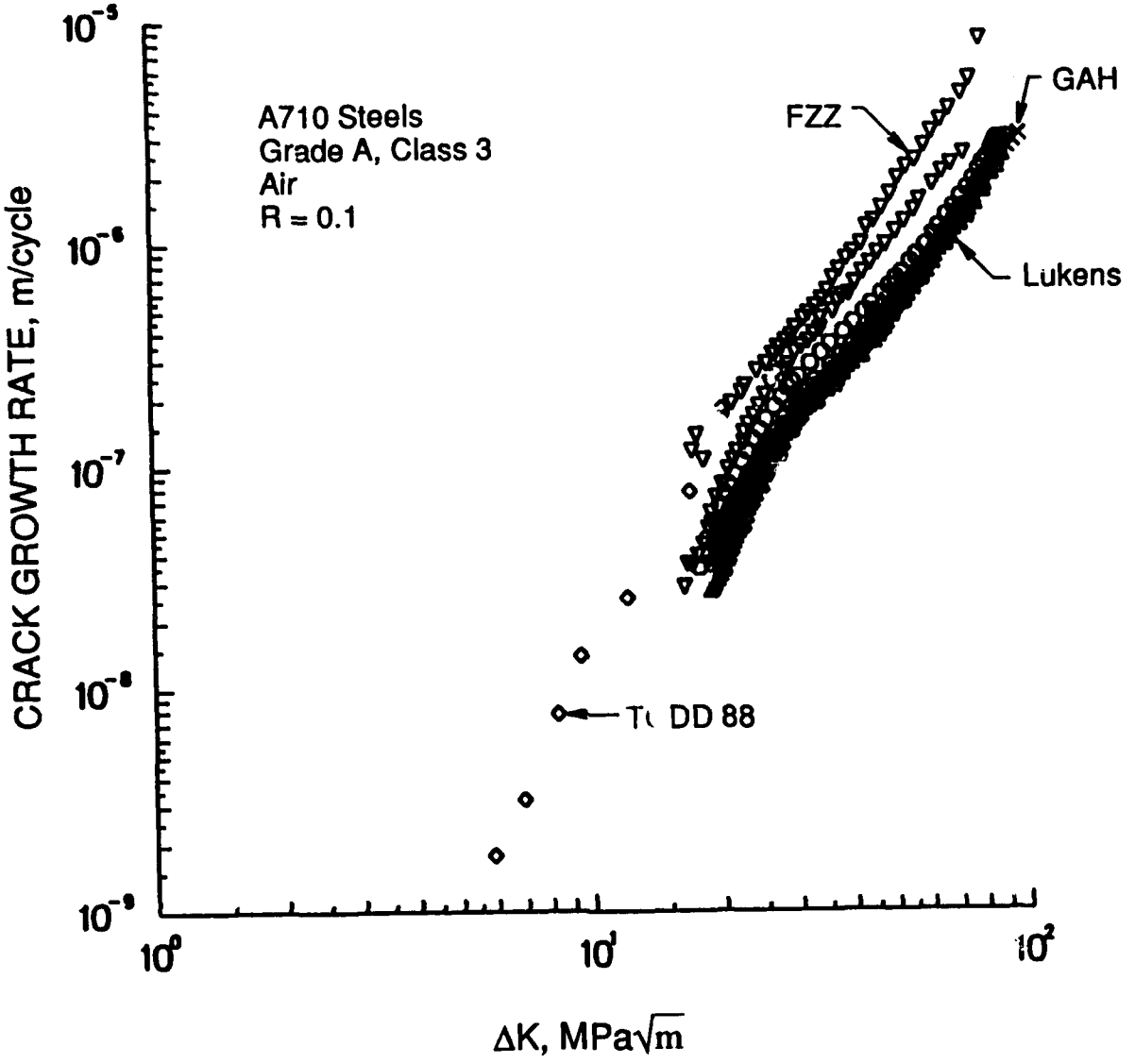

Figure 1. Fatigue crack growth data of A710 steels. Sources of data are Montemarano, et al. [1] (FZZ and GAH), Wilson, et al. [5], and Todd, et al. [7].

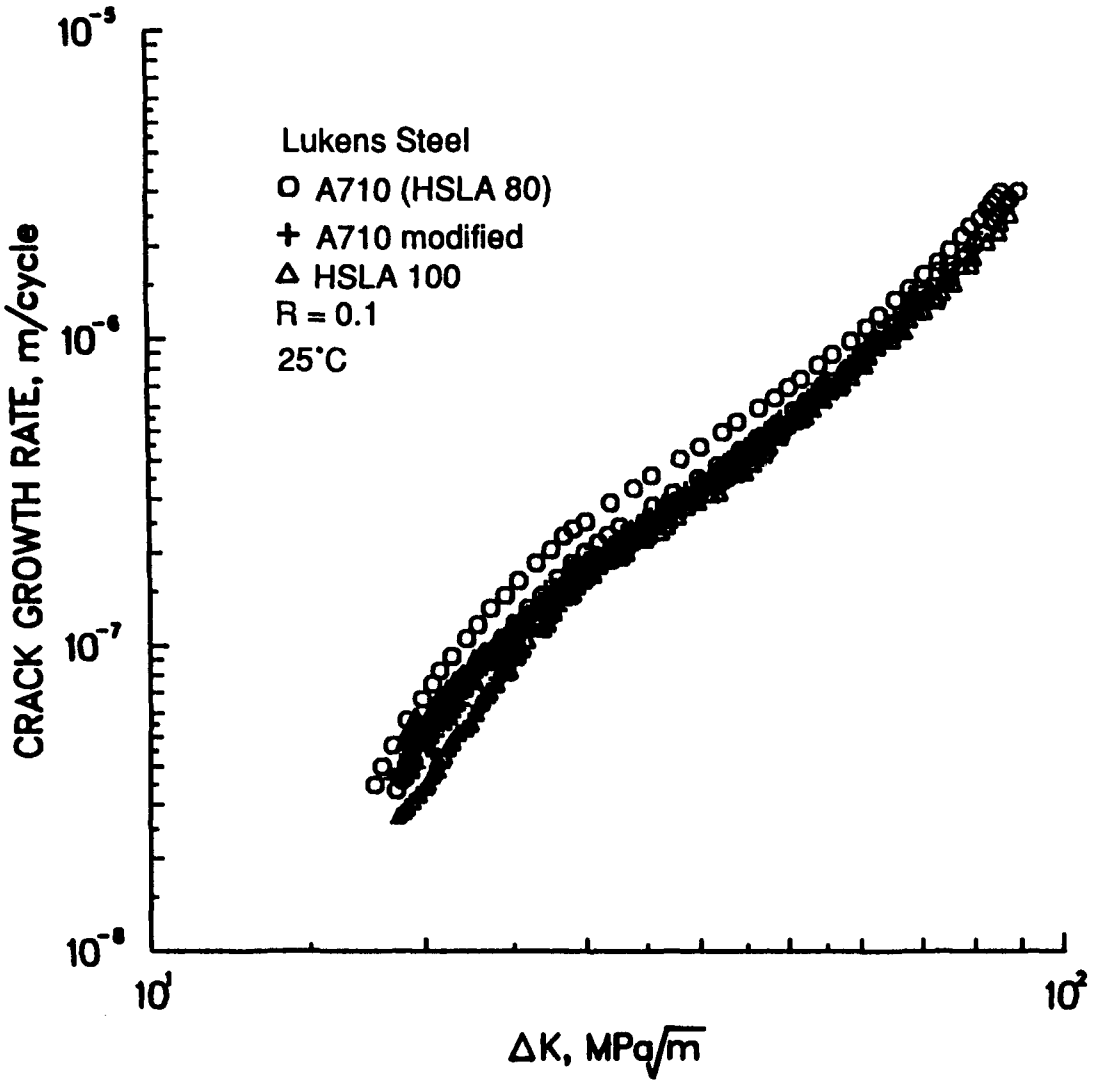

Figure 2. Comparison of fatigue crack growth data of A710 [5], A710 modified [5], and HSLA 100 steels [15].

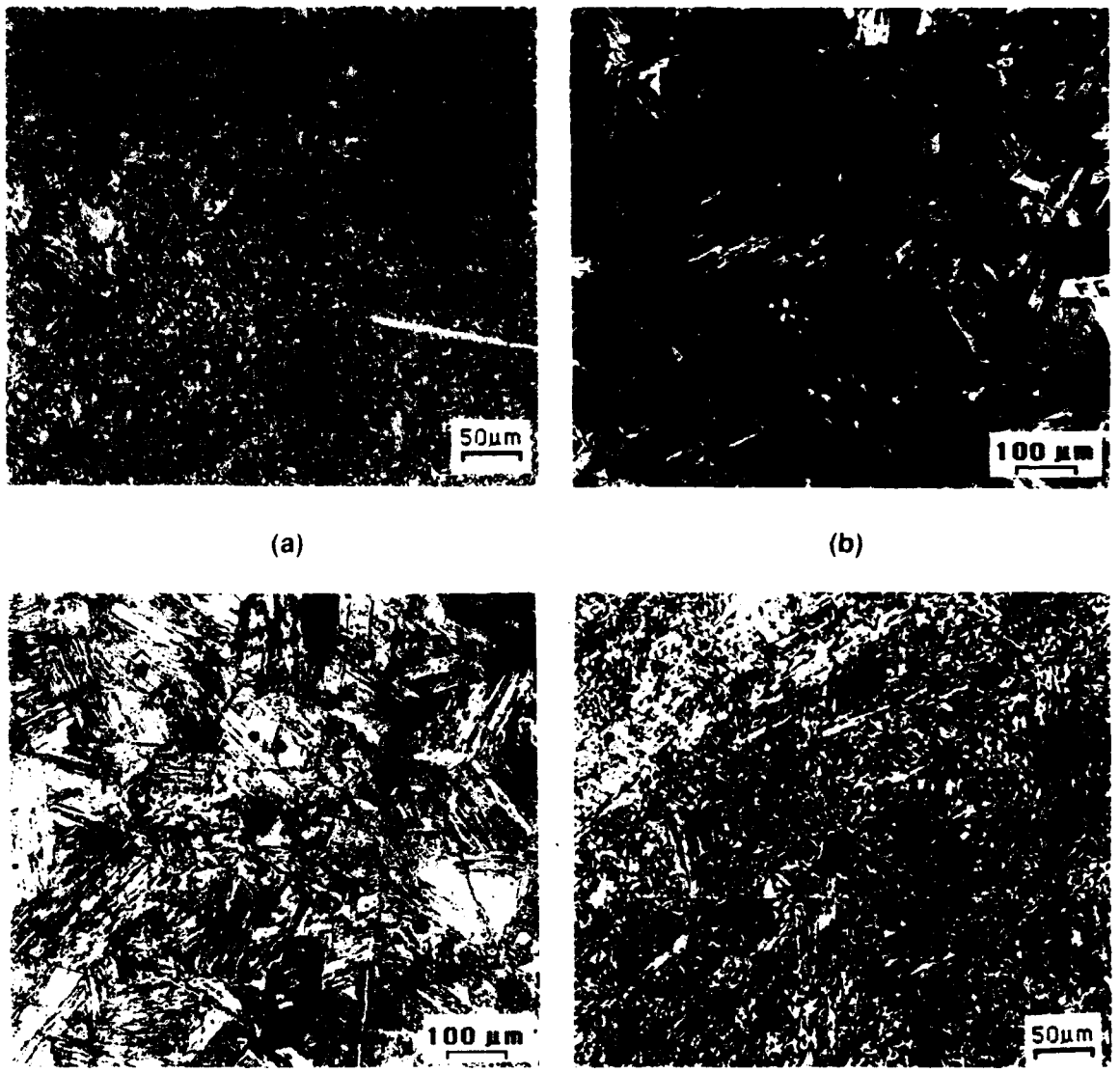

Figure 3. Microstructures of materials tested in fatigue. (a) as-received, sp. 353, (b) HT#2, sp. 357, (c) HT#3, sp. 358, and (d) weld, sp. 359.

FZZ

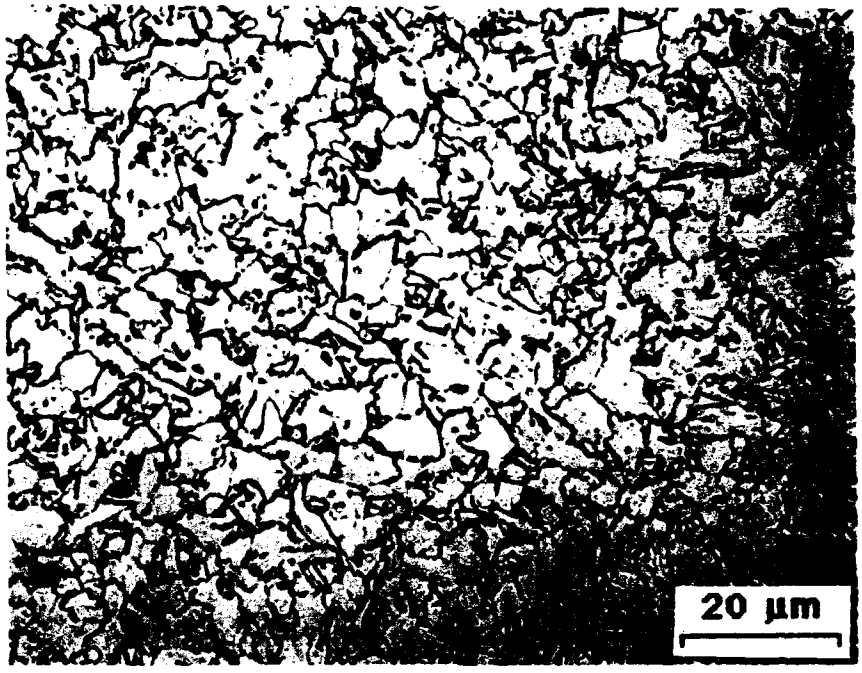

(a)

GAH

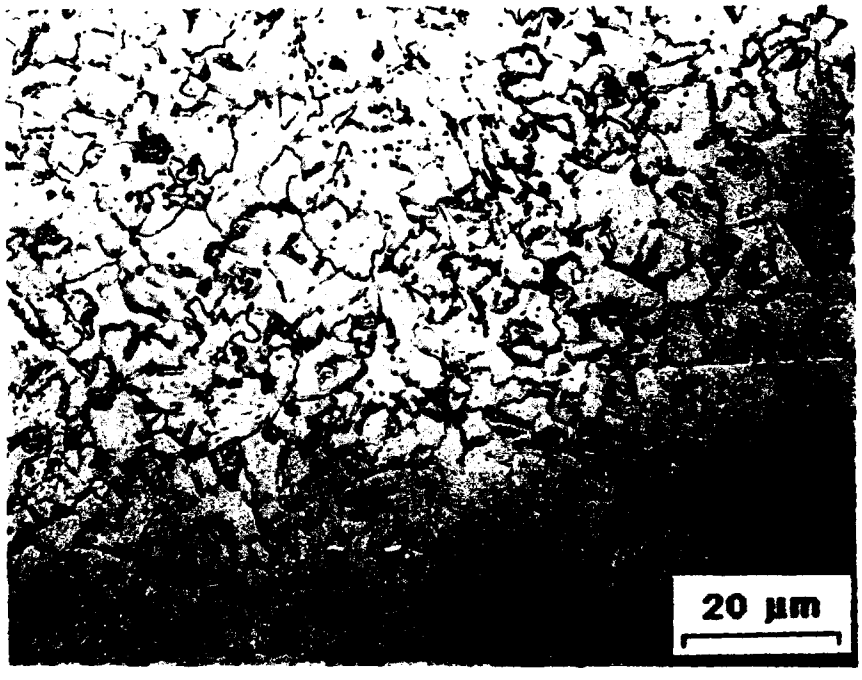

(b)

Figure 4. Microstructures of HSLA 80 steels from NTNSRDC: (a) FZZ plate, and (b) GAH plate.

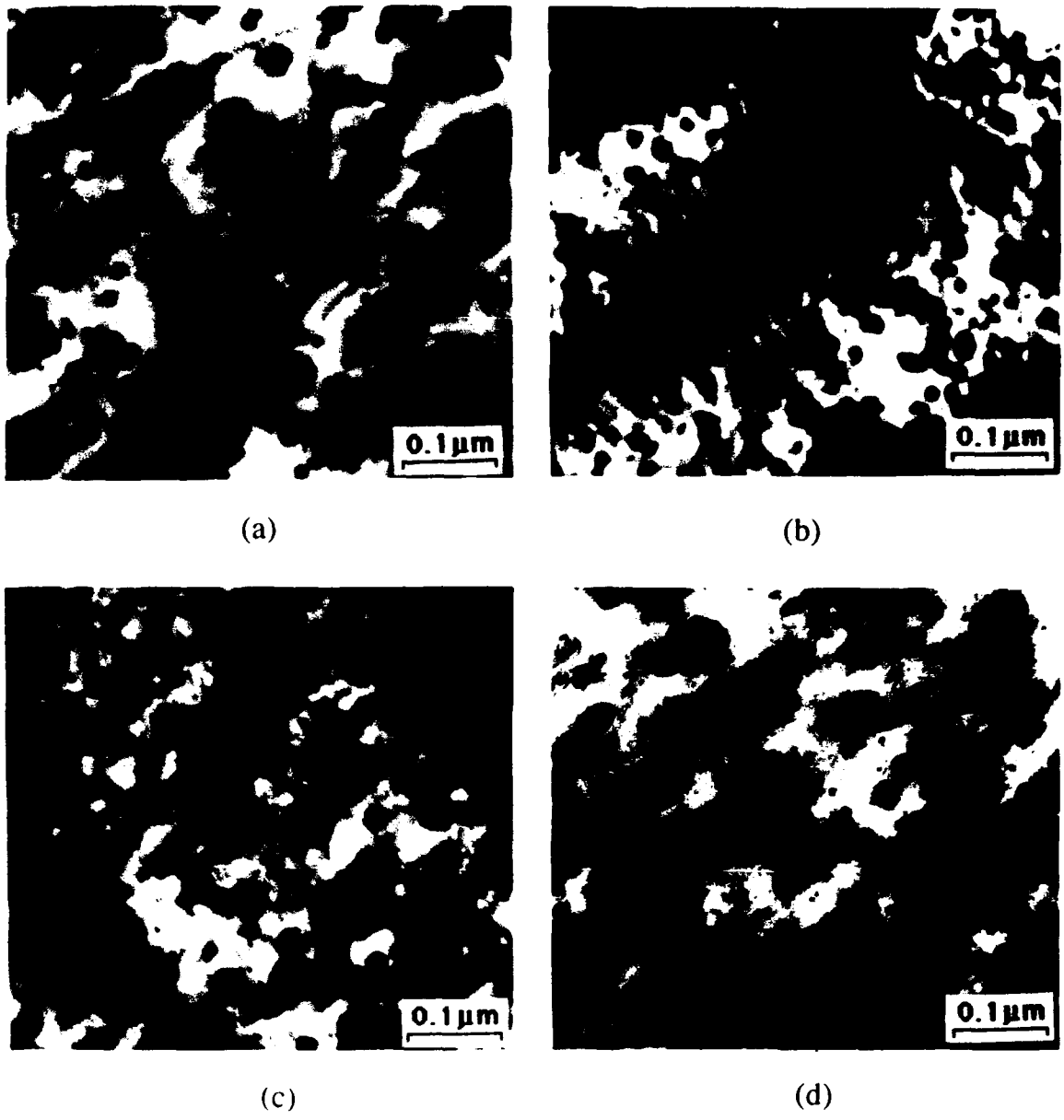

Figure 5. TEM micrographs showing ε-copper precipitates in HSLA 80 steels: (a) as-received, (b) HT#2, (c) HT#3, and (4) weld.

(a)

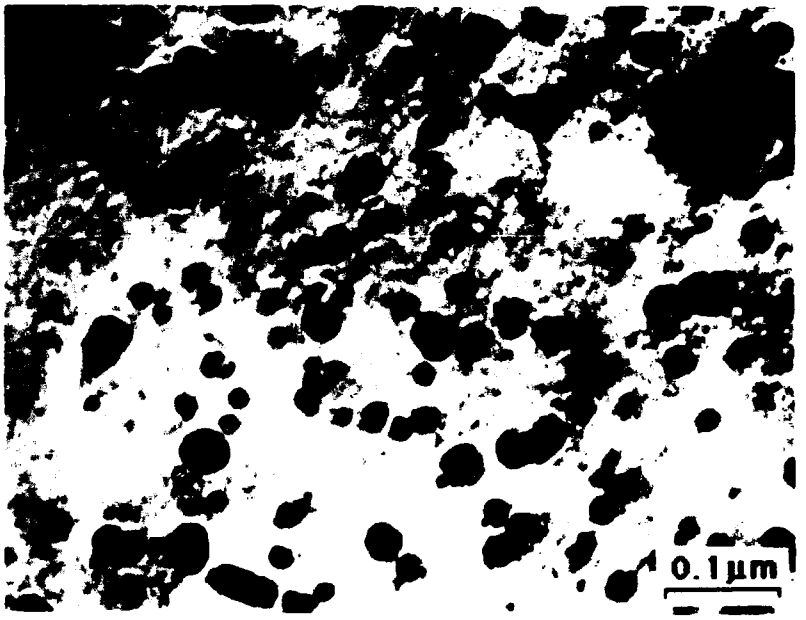

(b)

Figure 6. TEM micrographs showing fine ε-copper precipitates in FZZ (a) and coarse ε-copper precipitates in GAH (b).

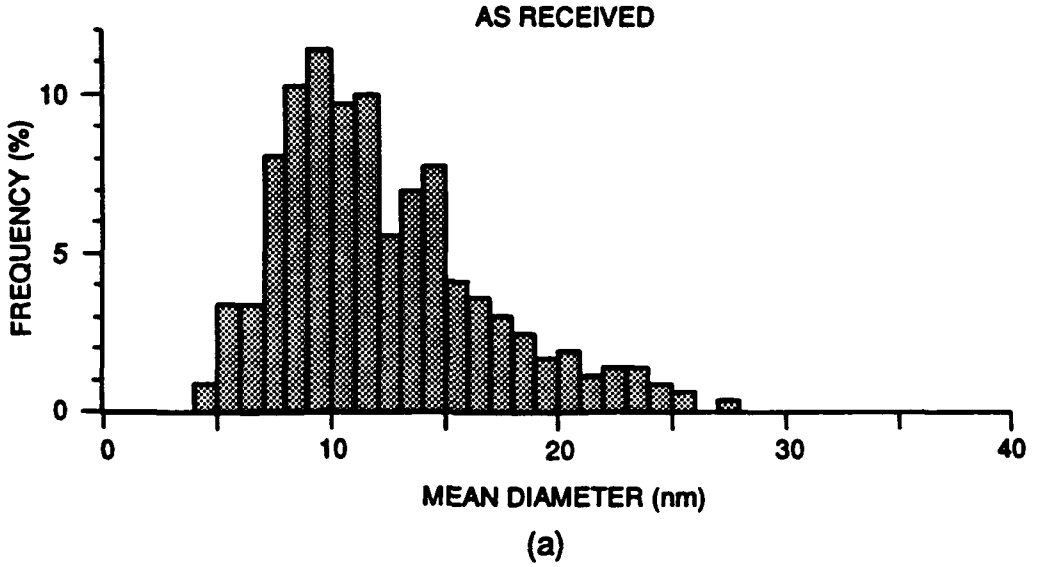

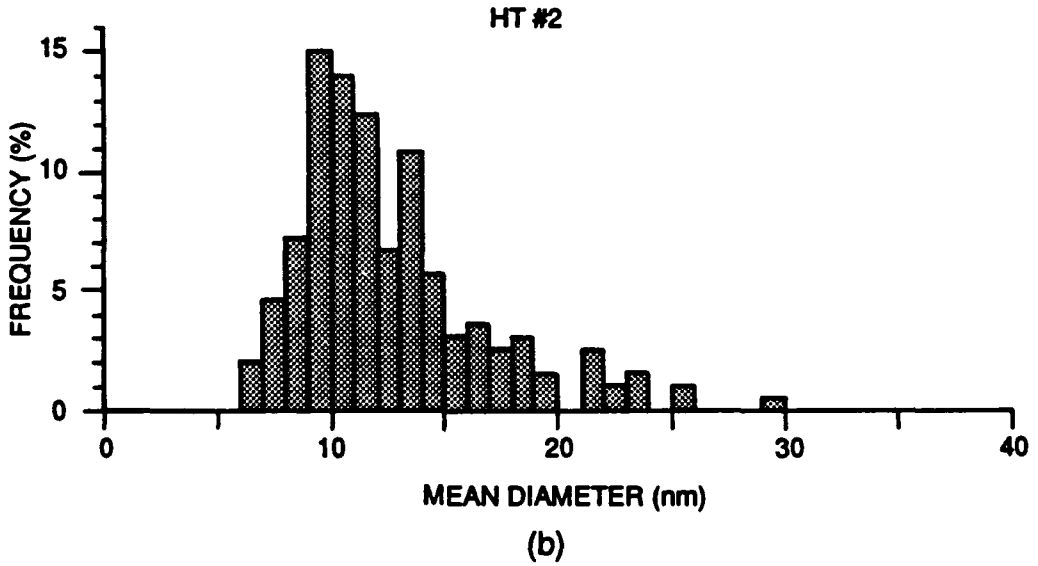

Figure 7. Distribution of ε-copper precipitates in HSLA steels: (a) as-received, (b) HT#2, (c) HT#3, and (d) weld.

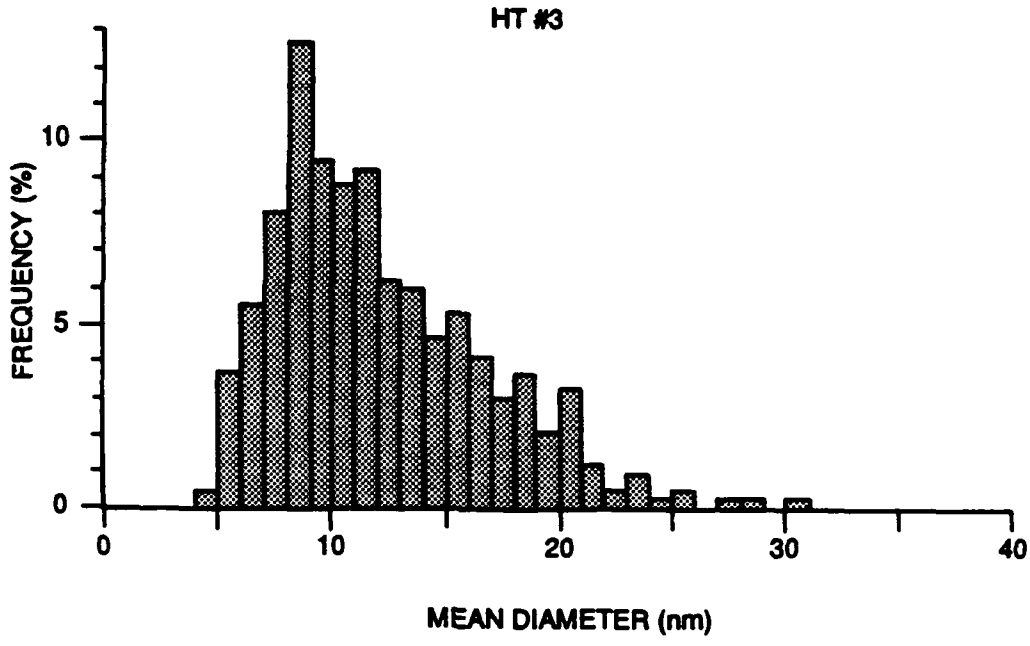

(c)

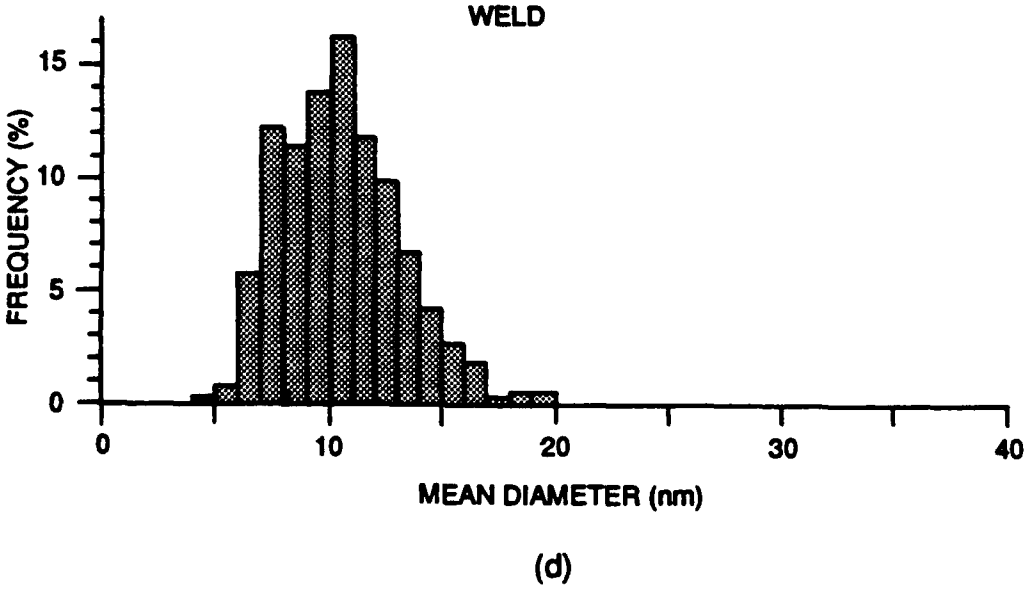

(d)

Figure 7. Distribution of ε-copper precipitates in HSLA steels: (a) as-received, (b) HT#2, (c) HT#3, and (d) weld (Con't).

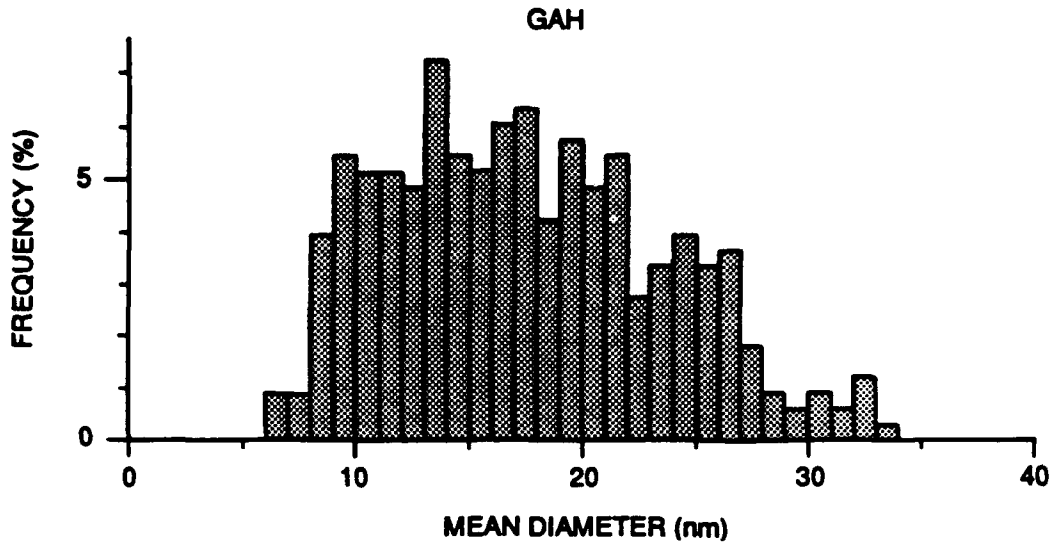

(a)

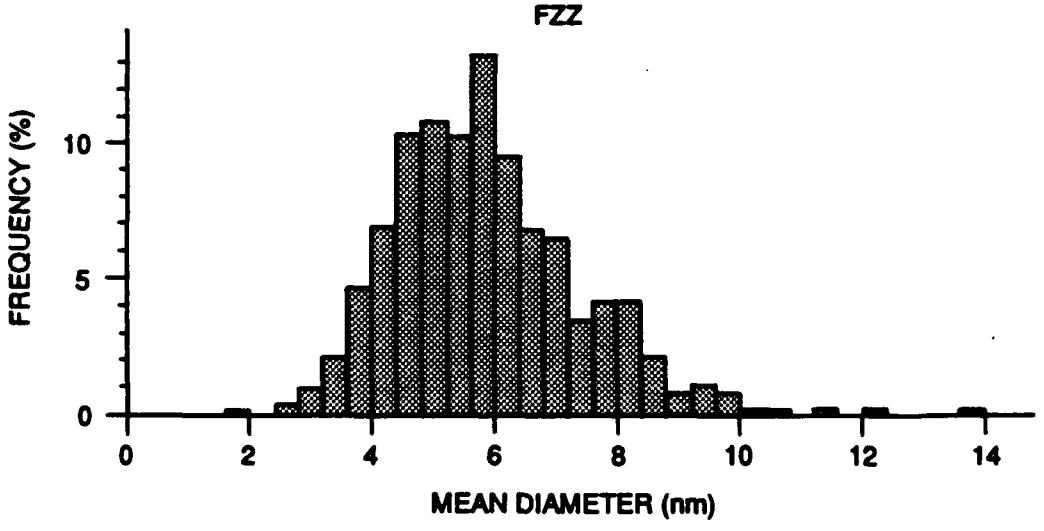

(b)

Figure 8. Distribution of ε-copper precipitates in HSLA 80 specimens from NTNSRDC: (a) GAH plate, and (b) FZZ plate.

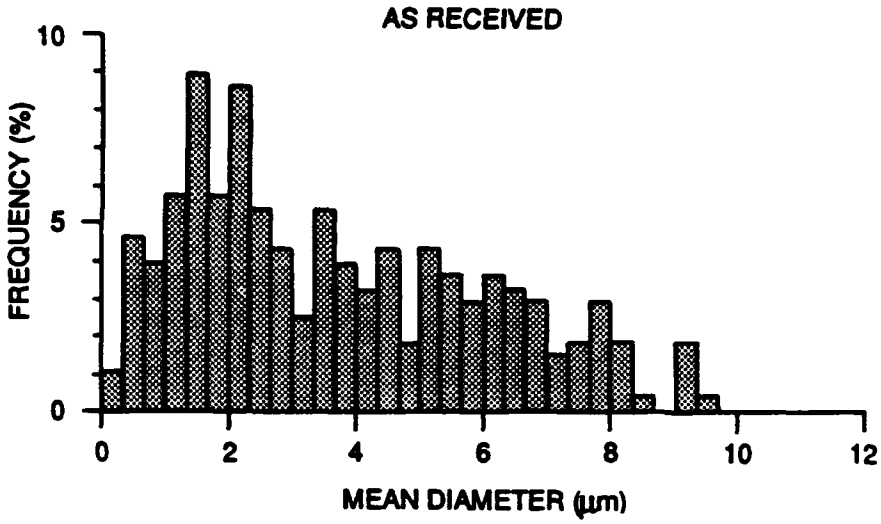

Figure 9. Grain size distribution in the as-received HSLA 80 plate.

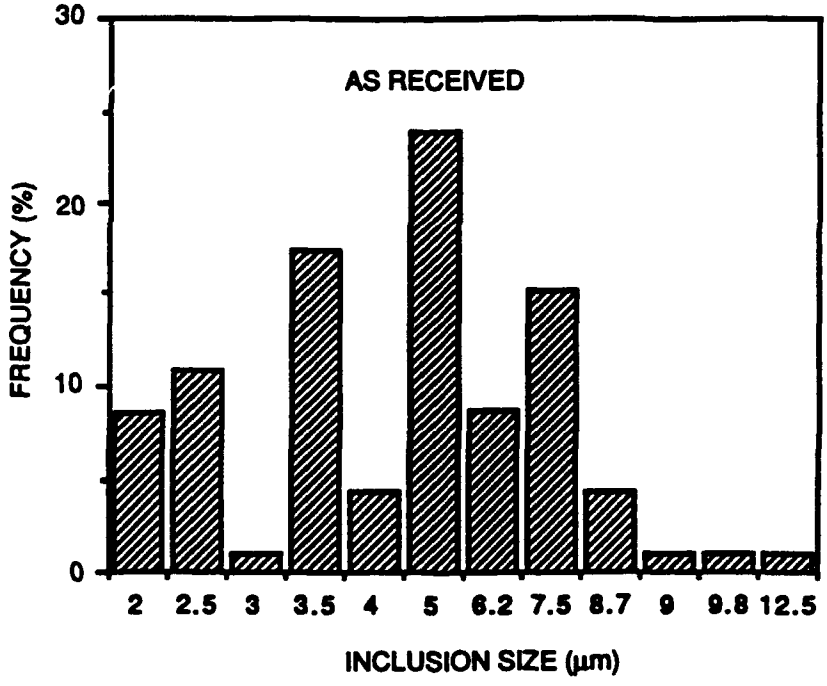

Figure 10. Inclusion size distribution in the as-received HSLA 80 plate.

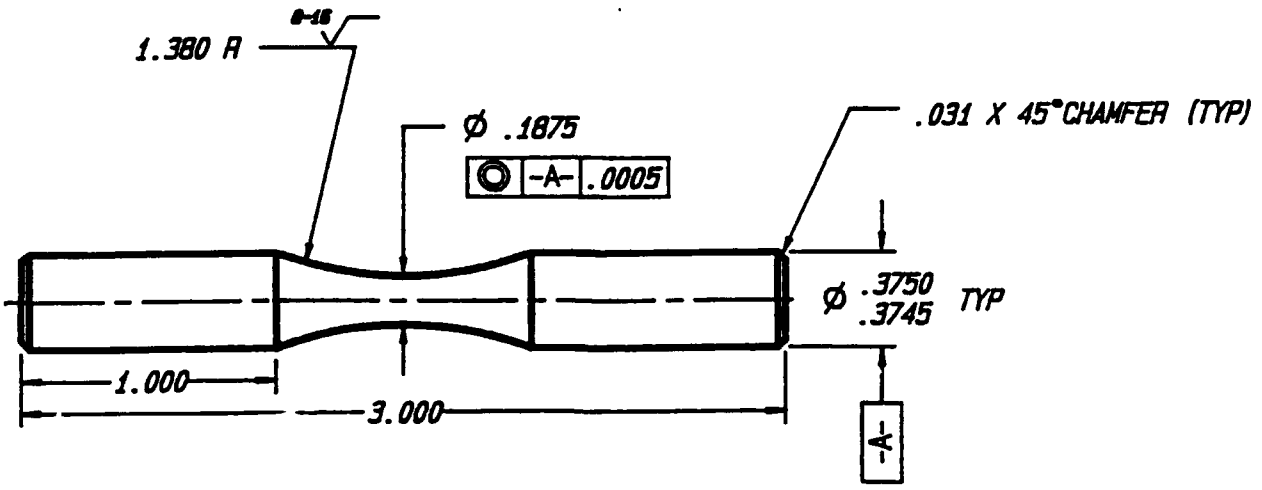

NOTE:
1. USE LOW STRESS MACHINING IN GAGE SECTION.
2. SMALL CENTERS ARE PERMISSIBLE.

Figure 11. Rotating beam specimen used for small crack growth study.

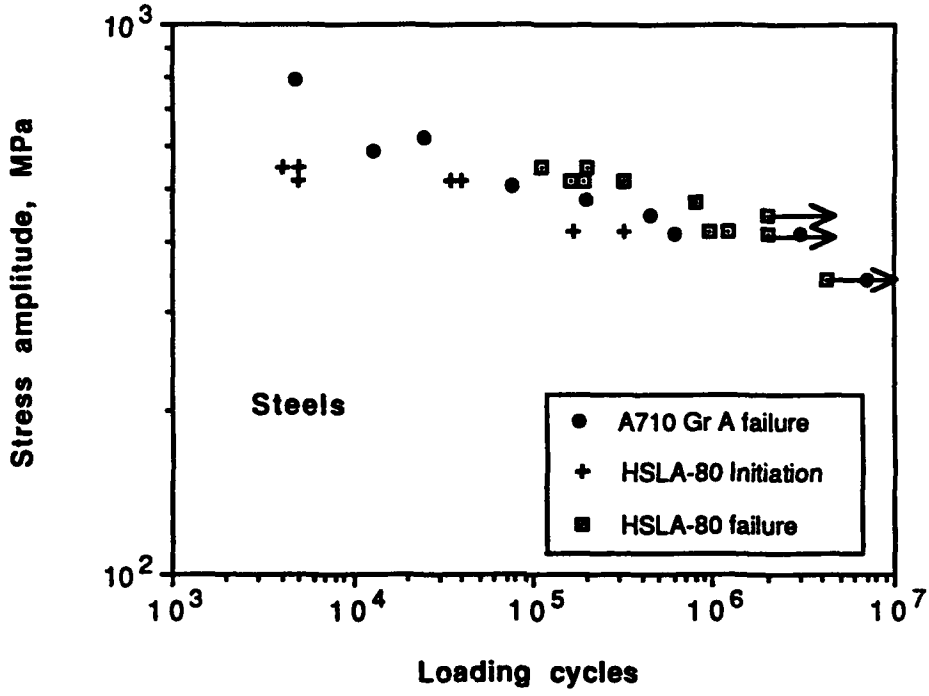

Figure 12. Stress-cycles to crack initiation and growth to 2-mm length. Data points with arrows are for specimens that did not initiate cracks.

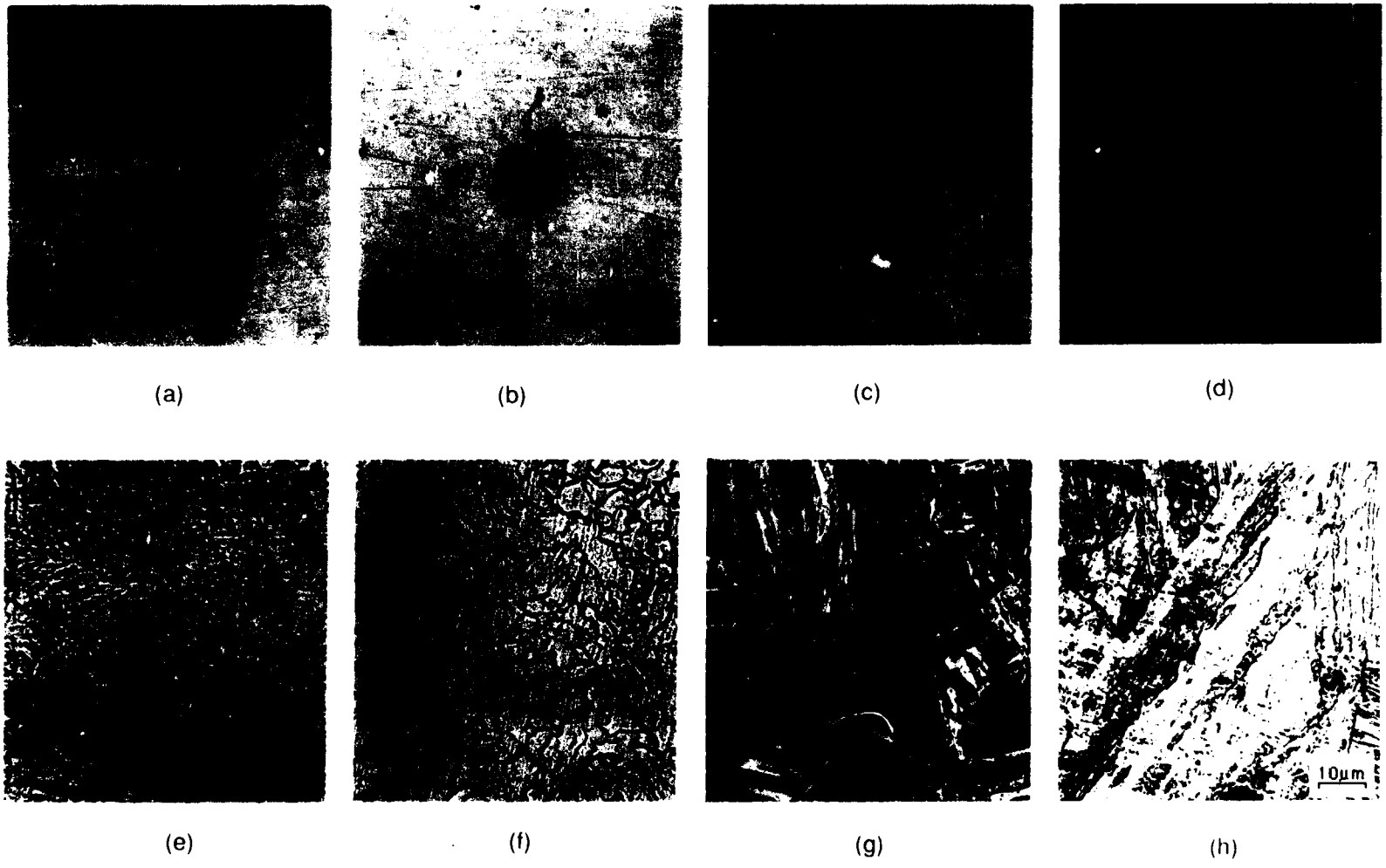

Figure 13. The relationship between microstructure and crack initiation sites: (a)-(d) show microcracks near initiation; (e)-(h) show microstructures of the same scale as the upper photographs. (a) and (e) as-received microstructure; (b) and (f) HT#1, sp. 350 (to cause grain growth); (c) and (g) HT#2, sp. 357, and (d) and (h) HT#3, sp. 358.

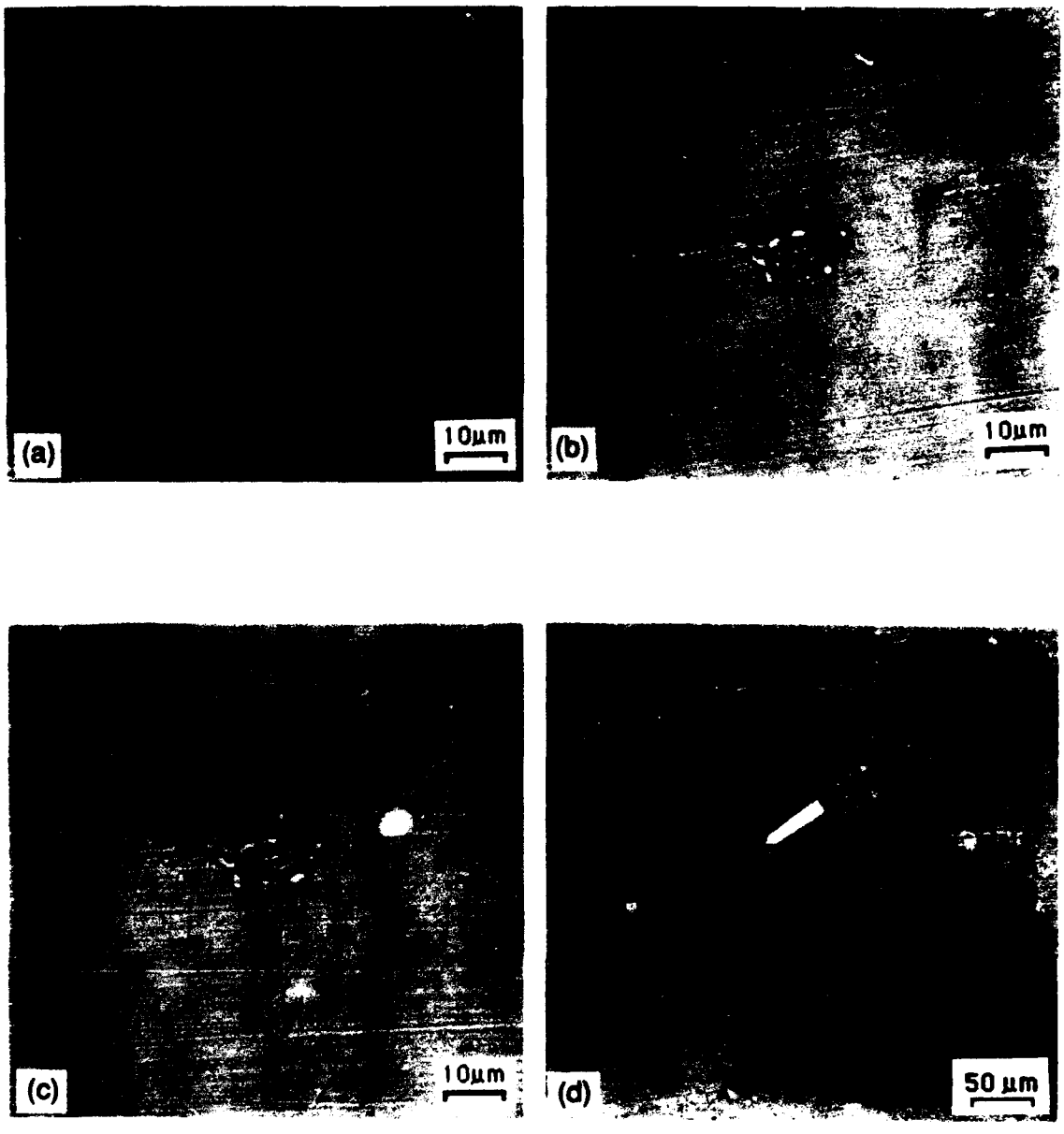

Figure 14. Crack initiation and growth sequence, as-received, sp. 353. (a) 26 kcy, (b) 30 kcy, (c) 70 kcy and (d) 170 kcy.

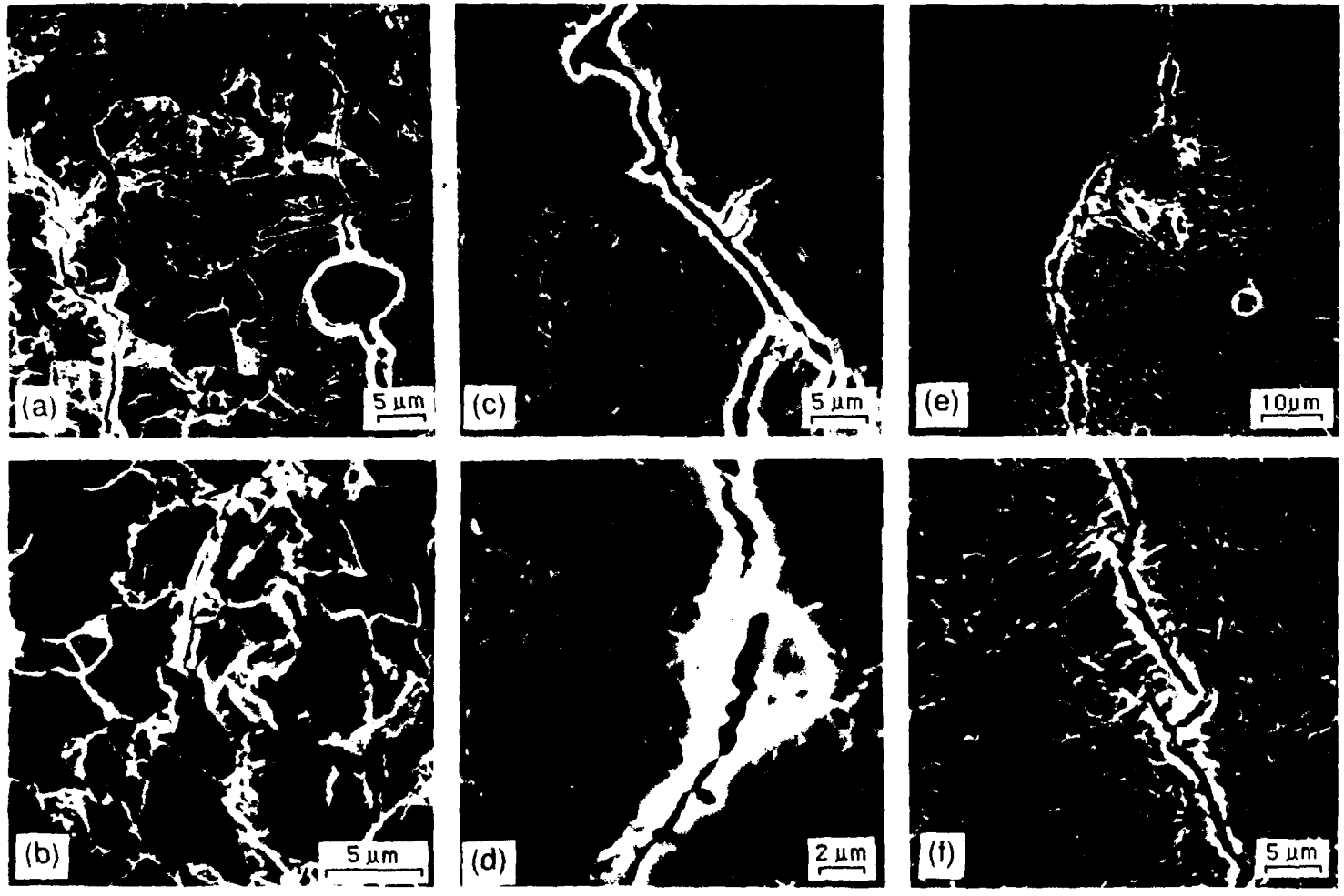

Figure 15. Crack path in relation to microstructural features. (a,b) as-received (Navy plate), (c,d) sp. 347, as-received (Lehigh plate), (e,f) sp. 353, and weld, sp. 359.

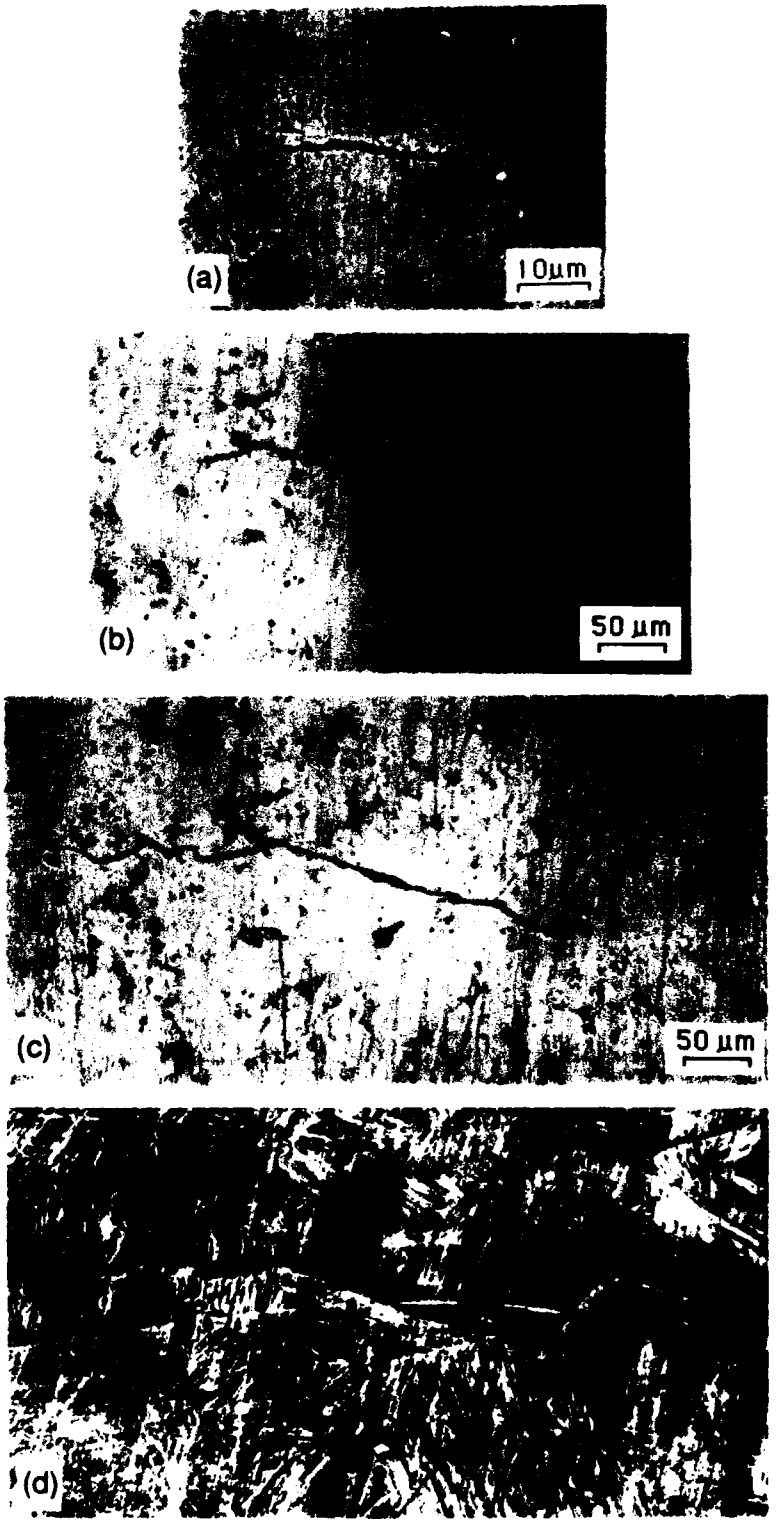

Figure 16. Crack initiation and growth sequence, HT#3, sp. 358: (a) 70 kcy, (b) 140 kcy, (c) 180 kcy, and (d) 180 kcy after etching. Stress axis vertical.

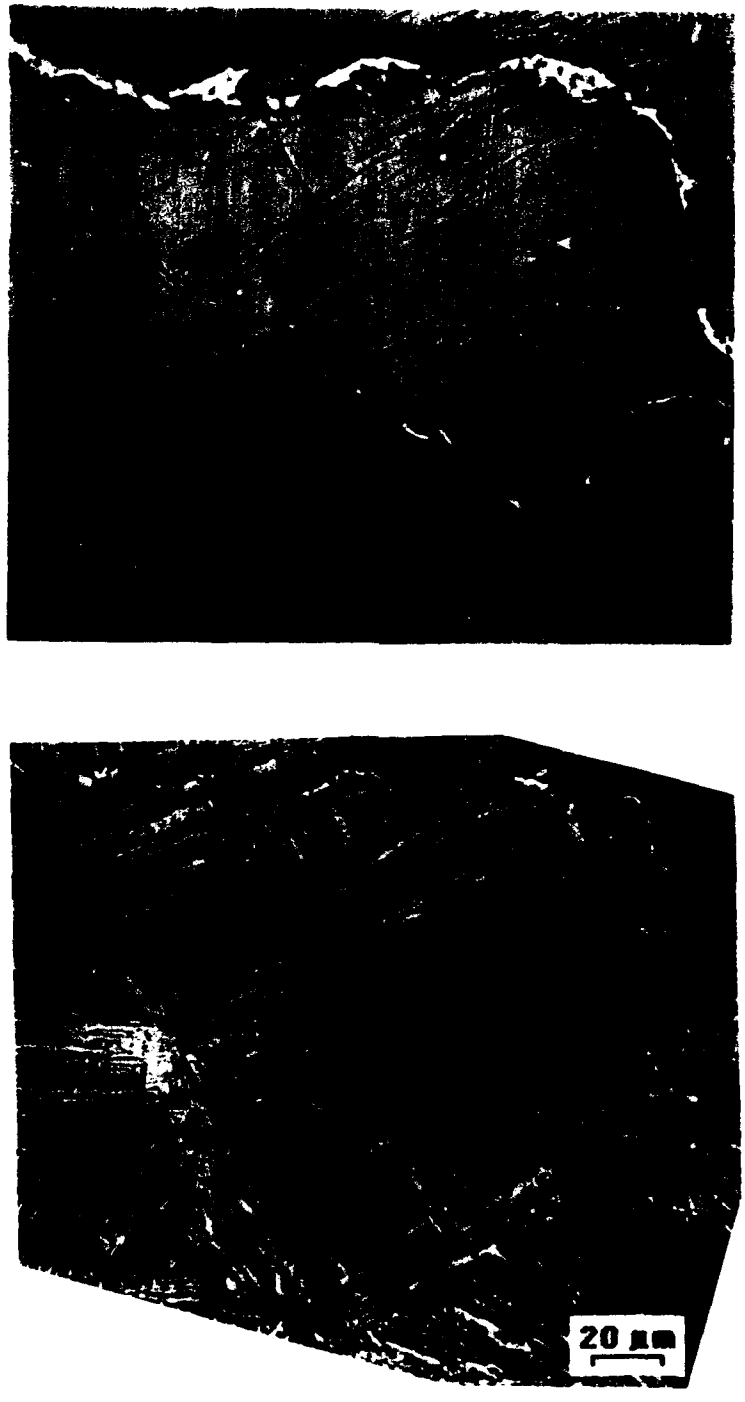

Figure 17. Crack path in relationship to microstructure, HT#2, sp. 357 after 110 kcy. Before and after etching. Stress axis vertical.

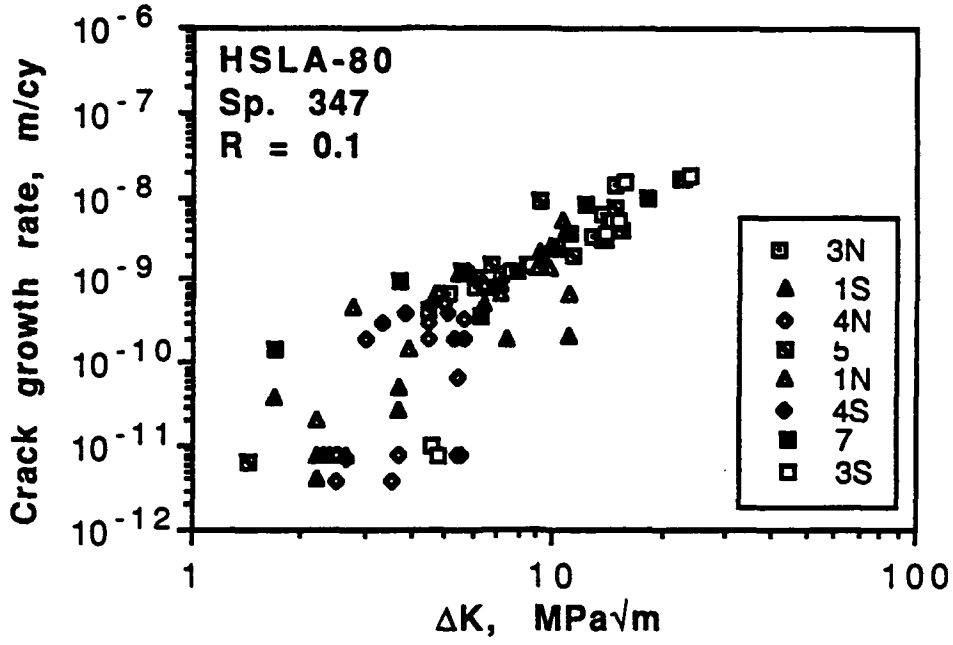

Figure 18. Fatigue crack growth rate for as-received material (Navy plate) from 3-point bend bar test, sp. 347.

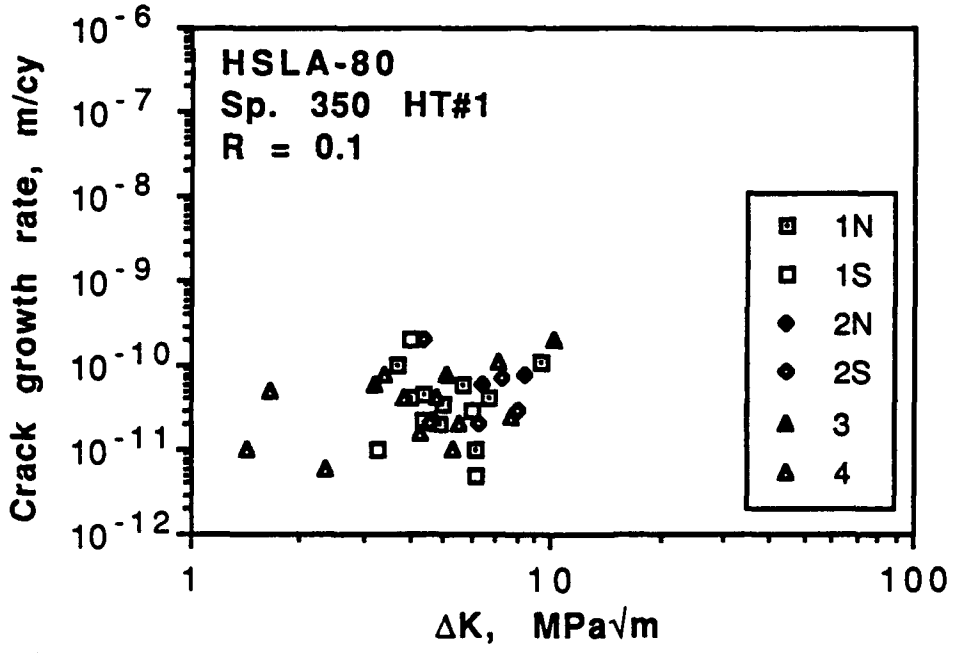

Figure 19. Fatigue crack growth rate for HT#1 (Navy plate) from 3-point bend bar test, sp. 350.

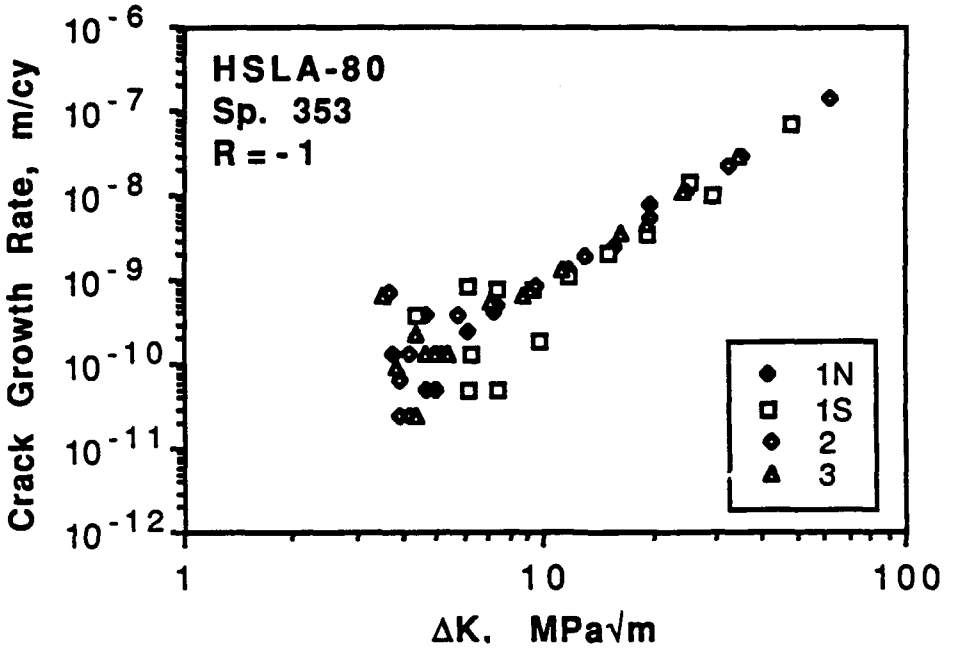

Figure 20. Fatigue crack growth rate for as-received material (Lehigh plate) from rotating beam test, sp. 353, stress amplitude = 550 MPa.

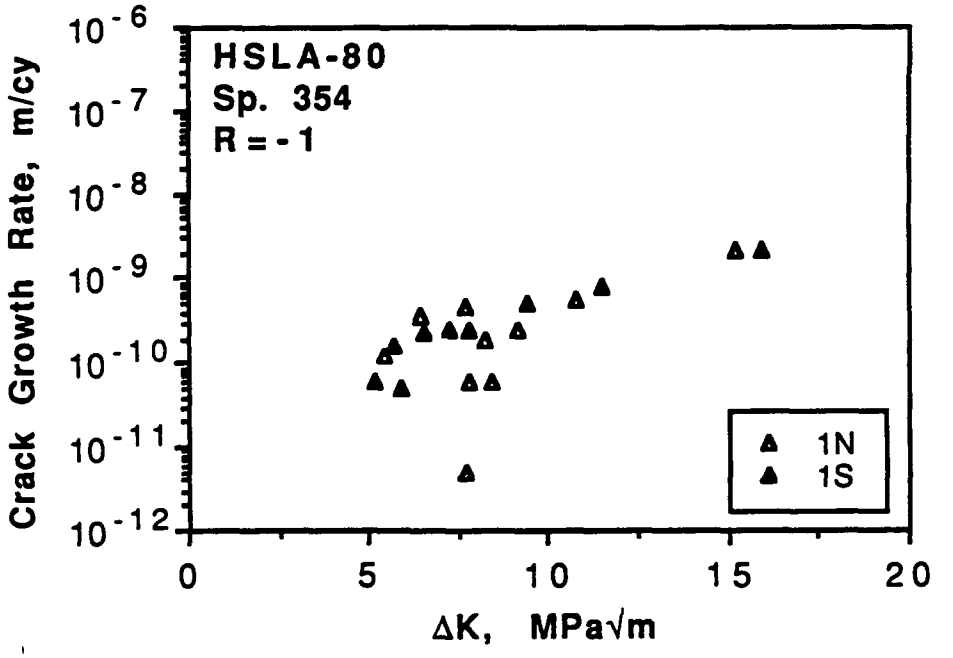

Figure 21. Fatigue crack growth rate for as-received material (Lehigh plate) from rotating beam test, sp. 354, stress amplitude = 520 MPa.

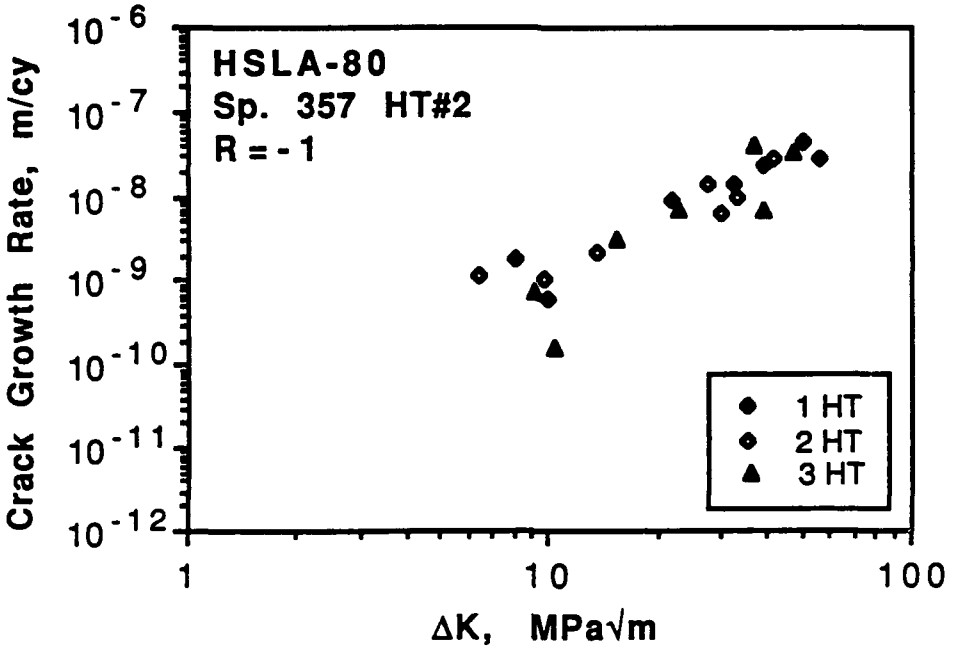

Figure 22. Fatigue crack growth rate, rotating beam test, for sp. 357, HT#2.

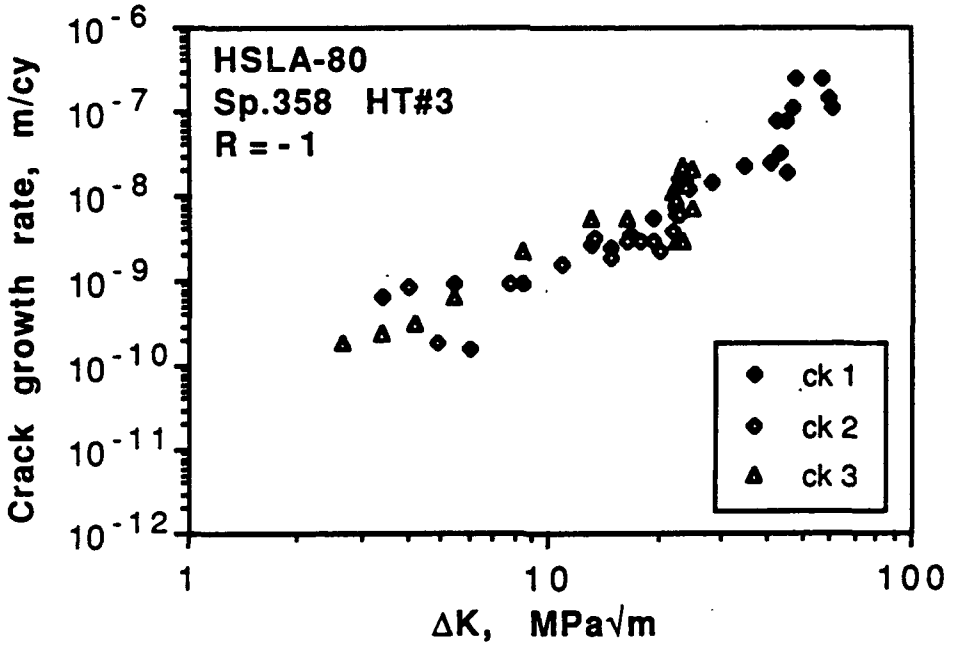

Figure 23. Fatigue crack growth rate, rotating beam test, for sp. 358, HT#3.

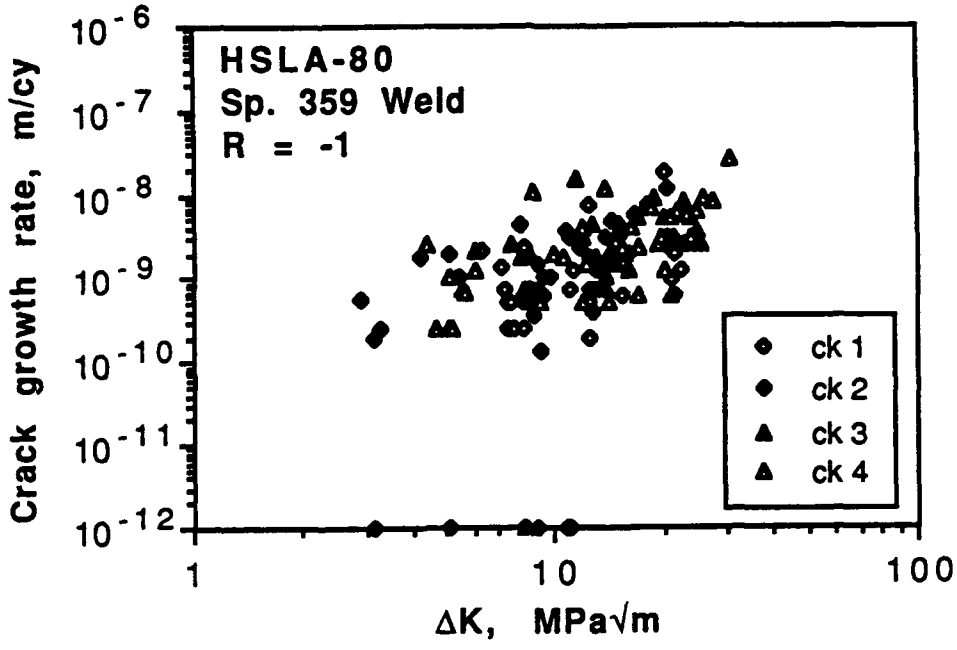

Figure 24. Fatigue crack growth rate, rotating beam test, for sp. 359, weld metal.

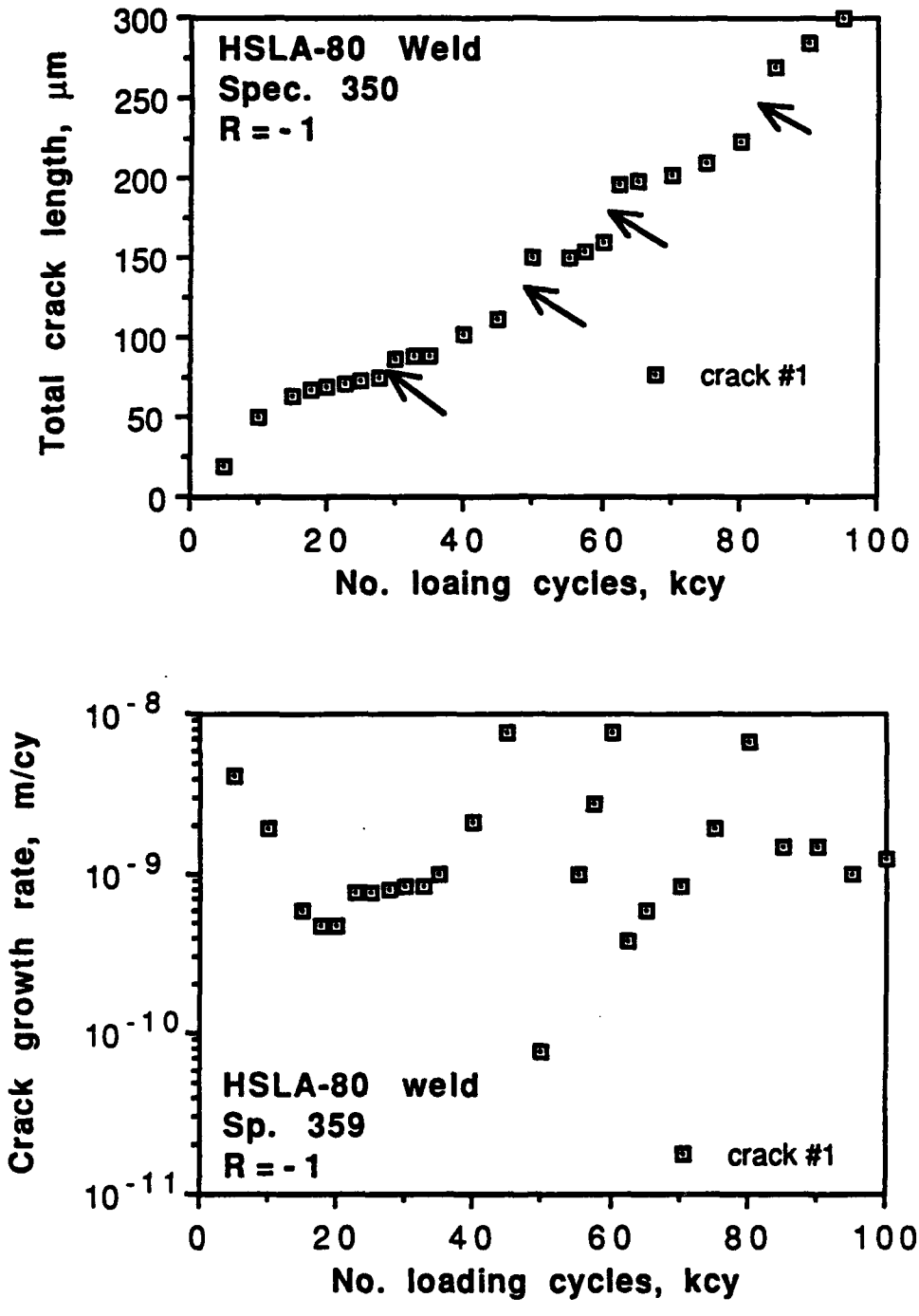

Figure 25. Weld metal specimen 359—comparison of the changes in crack length and crack growth rate as a function of loading cycles. Arrows indicate locations where cracks growth rate accelerated.

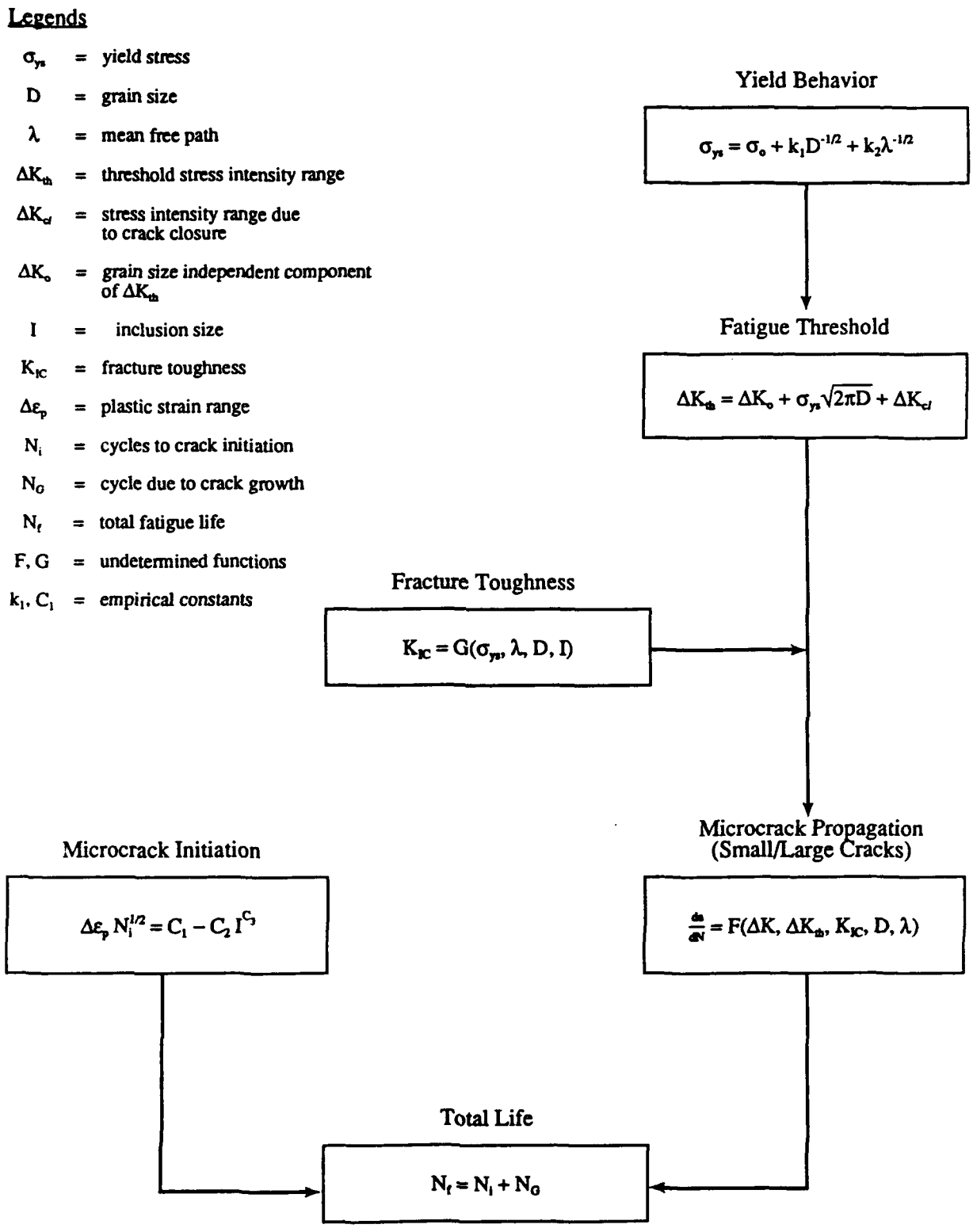

Figure 26. Flow chart showing the approach for developing microstructure\fatigue relationships for HSLA steels.

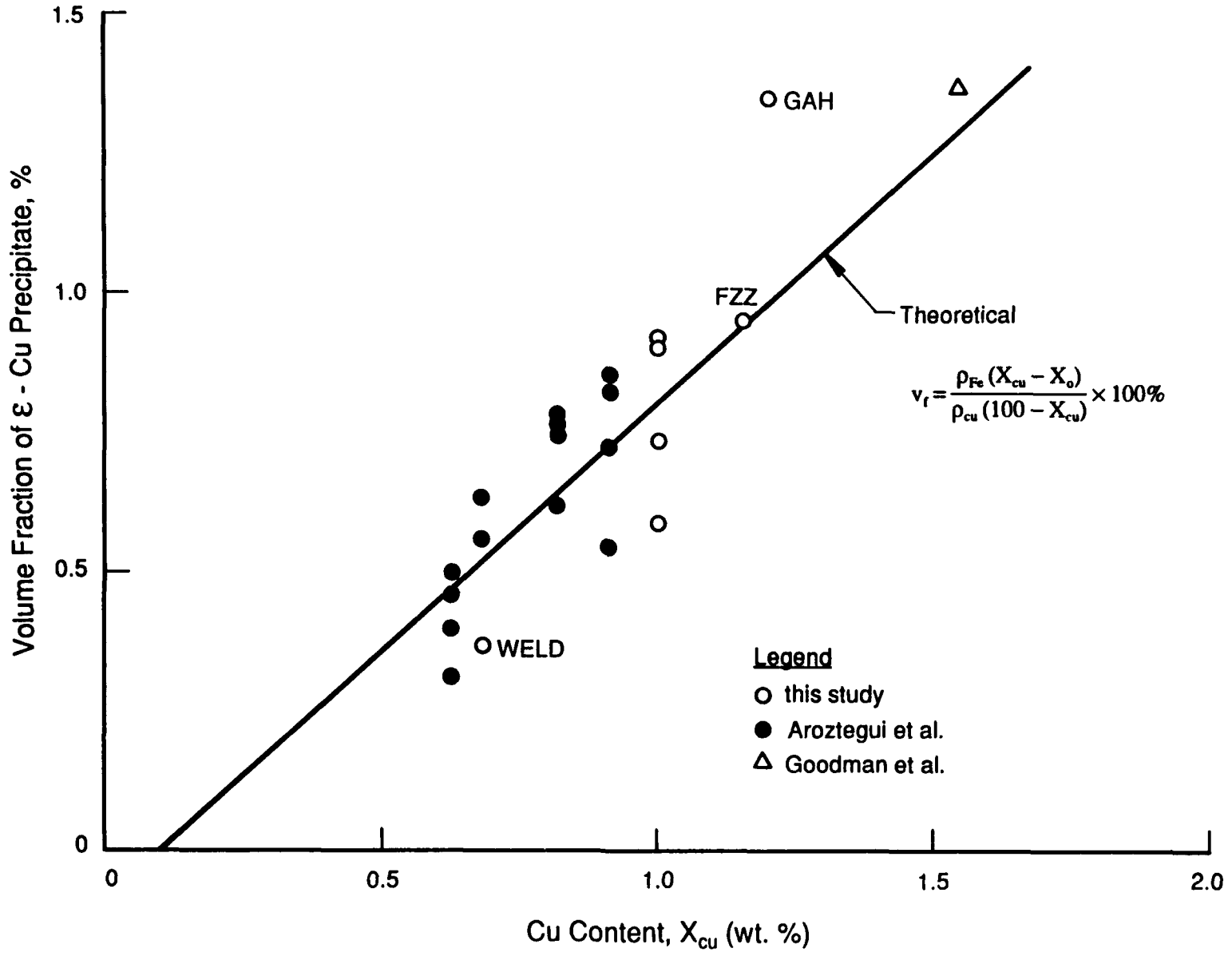

Figure 27. Theoretical and experimental results of volume fraction of ε-copper precipitates as a function of copper content in steels. The experimental results are from this study, Aroztegui, et al. [18], and Goodman, et al. [10].

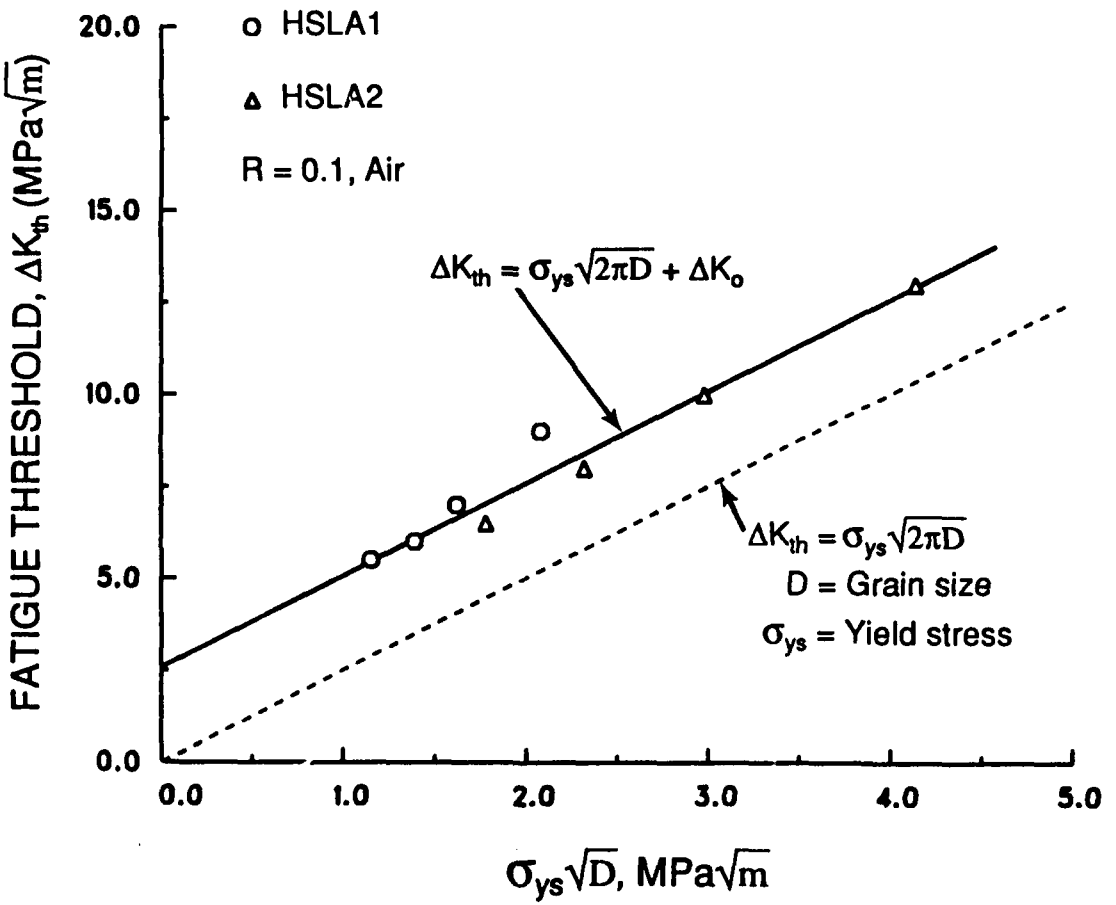

Figure 28. Theoretical and experimental relations between ΔK_{th} and $\sigma_{ys}\sqrt{D}$.

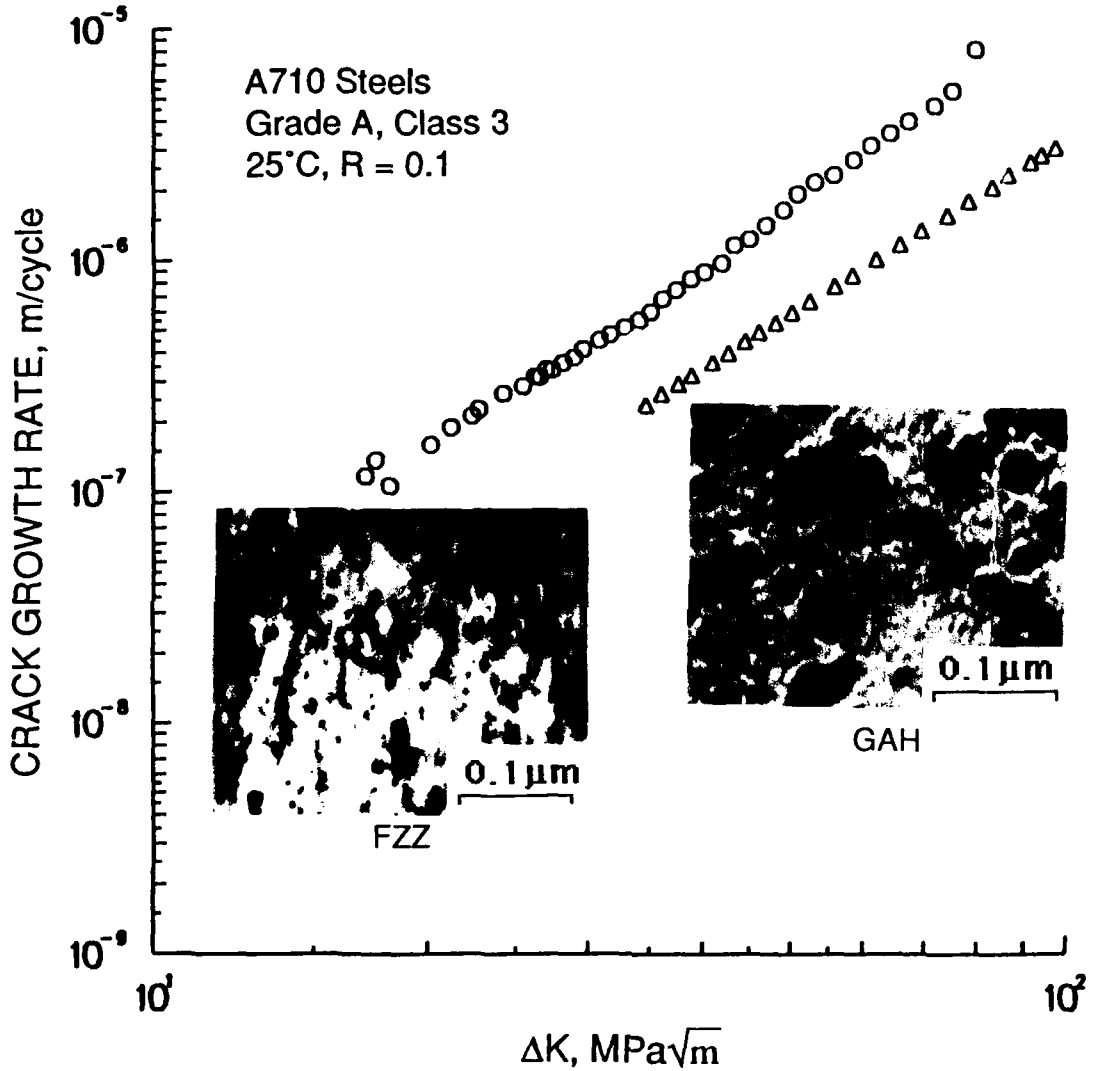

Figure 29. Dependence of fatigue crack growth rate on the size of ε-copper precipitates in FZZ and GAH plates.

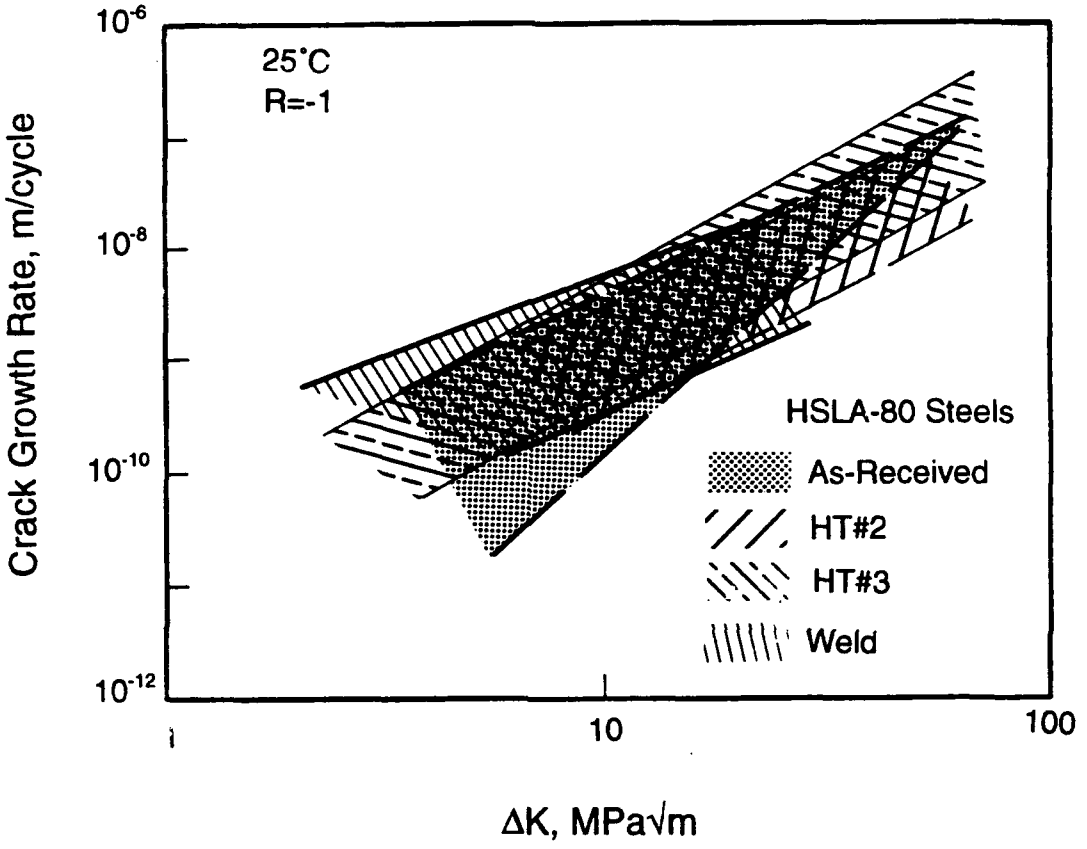

Figure 30. Comparison of fatigue crack growth responses of microcracks in HSLA-80 steels and weld.